ELSEVIER

Chemical Geology 227 (2006) 184–213

CHEMICAL GEOLOGY
INCLUDING
ISOTOPE GEOSCIENCE

www.elsevier.com/locate/chemgeo

Origins of CO_2 in permian carbonate reservoir rocks (Zechstein, Ca2) of the NW-German Basin (Lower Saxony)

M. Fischer [a], R. Botz [a,*], M. Schmidt [a], K. Rockenbauch [b], D. Garbe-Schönberg [a], J. Glodny [c], P. Gerling [d], R. Littke [e]

[a] *Institut f. Geowissenschaften, Universität Kiel, Olshausenstr. 40, 24118 Kiel, Germany*
[b] *ExxonMobil Production GmbH, Riethorst 12, 30659 Hannover, Germany*
[c] *GeoForschungsZentrum Potsdam, Telegraphenberg C2, 14473 Potsdam, Germany*
[d] *Bundesanstalt für Geowissenschaften und Rohstoffe, PF 510153, 30631 Hannover, Germany*
[e] *Lehrstuhl f. Geologie, Geochemie und Lagerstätten d. Erdöls und d. Kohle, RWTH Aachen, Lochnerstr. 4-20, 52056 Aachen, Germany*

Received 14 March 2005; received in revised form 7 September 2005; accepted 15 September 2005

Abstract

Permian carbonate reservoir rocks (Stassfurt-Carbonate) of the CO_2-province (Lower Saxony Basin, NW Germany) are locally characterised by high amounts of CO_2 leading to serious problems on exploration. In order to receive information on the major CO_2 sources and CO_2 migration and accumulation processes mineralogical, geochemical and stable isotope analyses (^{13}C, ^{18}O) were carried out on authigenic precipitations within the Stassfurt carbonate rocks (Ca2).

These rocks contain early diagenetic (e.g., formed in soft sediment) carbonate minerals (calcite, dolomite) and anhydrite in concretions and small cracks. In addition, large (up to 2 cm wide) carbonate-cemented fractures formed in solid Ca2 rocks. Semi-quantitative estimates of the diagenetic mineral content showed variations between the investigated rock cores. Nine out of 12 Ca2 rock cores are derived from wells situated in the area of modern CH_4-rich reservoirs and have distinct fracture systems developed. In contrast, the other three rock cores are from wells characterised by CO_2-rich reservoirs and lack fractures of similar thickness. The assumed relationship between tectonically induced fractures and the gas content of the Ca2 reservoir rocks implies CO_2 degassing of the Ca2 rocks at approximately 102 °C to ~150 °C (assumed $\delta^{18}O_{pore\ water}$ variation from 0‰ to +4‰ SMOW).

REE distribution indicates at least three types of fracture- and crack-filling carbonates. Two carbonate generations formed from evolving diagenetic pore waters whereas one type reflects carbonate formation under hydrothermal influence. The ages of these cementations derived from Rb/Sr and U/Pb isotope analyses indicate their formation during late stage of/or after the inversion of the Lower Saxony Basin in Late Cretaceous times.

The stable carbon isotope composition of the authigenic carbonate minerals reflects at least two carbon source endmembers available during diagenesis. Whereas many early-formed carbonates are related to the Permian ^{13}C-rich carbon source, those carbonates which precipitated or recrystallised during early to late stage diagenesis and/or were induced by local tectonic events incorporated ^{12}C-enriched CO_2 from organic degradation processes.

The stable oxygen isotope values of authigenic carbonates probably still reflect low temperatures of mineral formation from Permian sea water (as it is assumed for "non" recrystallised carbonates) or late-stage high-temperature (up to ~150 °C) precipitation from sea water-derived pore waters which may have been locally influenced by ^{18}O-enriched fluids. However, most of the carbonate samples investigated are recrystallised (crystal enlargement of concretionary and fracture carbonate is observed) and

* Corresponding author. Tel.: +49 431 8802854; fax: +49 431 8804376.
E-mail address: rb@gpi.uni-kiel.de (R. Botz).

0009-2541/$ - see front matter
doi:10.1016/j.chemgeo.2005.09.014

hence, these carbonates are at least partly re-equilibrated (original ^{18}O-content reduced) with surrounding pore waters at elevated temperature.

Similar to the authigenic carbonate at least two sources may explain the concentration/carbon isotope relationship of modern CO_2 present in the Ca2 reservoir rocks. An organic-derived CO_2 endmember source ($\delta^{13}C$ near −20‰) is present in relatively low concentrations whereas large CO_2 concentrations derived from an endmember source with an isotope value near 0‰. Although the latter source is unknown such "heavy" CO_2 sources are most likely attributed to carbonate decomposition processes.

Keywords: Zechstein carbonate; Stable isotopes; Lower Saxony Basin; Carbon dioxide; Fracture mineralisation

1. Introduction

In Permian carbonate reservoir rocks (Stassfurt-Carbonate, Ca2) of the Lower Saxony Basin (LSB; Fig. 1a) locally high amounts of CO_2 are found. The gas situation in the so-called "CO_2-province" poses an additional uncertainty and risk for exploration activities because up to now no unambiguous relation between the amount of CO_2 and reservoir geological or geochemical parameters has been established. A reliable prediction for a specific prospective drill location is therefore very difficult to make.

The present work addresses the isotope geochemical relationship between authigenic carbonate minerals and related changes of CO_2 gas in reservoir rocks in order to understand the processes of CO_2 migration and accumulation in this area.

Carbonate sediments that are affected by dissolution, recrystallisation and/or cementation during rock formation record their diagenetic "history" by the mineral and geochemical composition of the carbonate components. This study was therefore based on mineralogical, geochemical, and in particular on stable isotope analyses (^{13}C, ^{18}O) of fracture- and cleat-filling minerals within the Stassfurt carbonate. They provide information on precipitation conditions (temperature, fluid composition) and major CO_2 source(s) during diagenesis reflecting CO_2 reservoir gases of at least two different origins.

1.1. Geological background

The area of investigation is located approximately 60 km north-west of Hannover (Fig. 1b,c) in the central part of the LSB, which represents an intra-plate crustal segment in NW Germany with a length of some 300 km and a width of about 60 km. It is a W–E striking trough at the southern end of the Zechstein Basin which is superimposed on the late Carboniferous Variscan foredeep crosscutting the older, northernmost fringe of the WSW–ENE striking Variscan orogenic front (Brink et al., 1992). The LSB subsided between the Pompeckj Block in the north and the Rhenish Massif in the south in Late Jurassic to Early Cretaceous times (Boigk, 1981). Two inversion phases during Upper Cretaceous and Lower Tertiary led to an uplift of the sediments (Betz et al., 1987). These tectonic activities were possibly associated with magmatic intrusions of the Bramsche, Vlotho and Uchte Massifs (Brink, 2002; Kockel et al., 1994), although there is new evidence that deep burial followed by large scale inversion created the high thermal maturity of the area (Petmecky et al., 1999).

The pre-salt basement is intensely structured by normal and reverse faults into a pattern of horst and graben structures as a result of extensional tectonics (Rockenbauch et al., 1998). The high blocks host North Germany's sourgas reservoirs (Kockel et al., 1994), which are bound to the 'Zechstein 2 Carbonate' or 'Ca2'. These carbonates are part of the "Basal Zechstein" consisting of the Werra-anhydrites (A1) situated below the Ca2 and the Stassfurt-anhydrites (A2) on top acting as a seal for the Ca2 reservoir (Fig. 1d; Strohmenger et al., 1996). The anhydrite-carbonate-anhydrite triplet forms the uppermost part of the pre-salt basement in NW Germany.

1.2. Stassfurt-Carbonate (Ca2)—reservoir rocks

The Ca2 can be subdivided into a number of facies types which represent specific palaeogeographic positions on the Zechstein carbonate shelf (Strohmenger et al., 1996). The Ca2 of the "Wiehengebirgsvorland" area is mainly developed in platform facies with adjacent slope mudstones in the south. The Ca2 platform facies is characterised by 14 subfacies types which all represent shallow subtidal to supratidal environments. The vertical stacking pattern of these subfacies usually displays two major shallowing-upward cycles and four subcycles. Each of the four small-scale cycles shows upward gradation from moderate to high energy subfacies into intertidal/supratidal subfacies (Strohmenger et al., 1993, 1996). The individual subfacies types and the distribution of grainy particles can be related to primary porosity types (Steinhoff and Strohmenger, 1996).

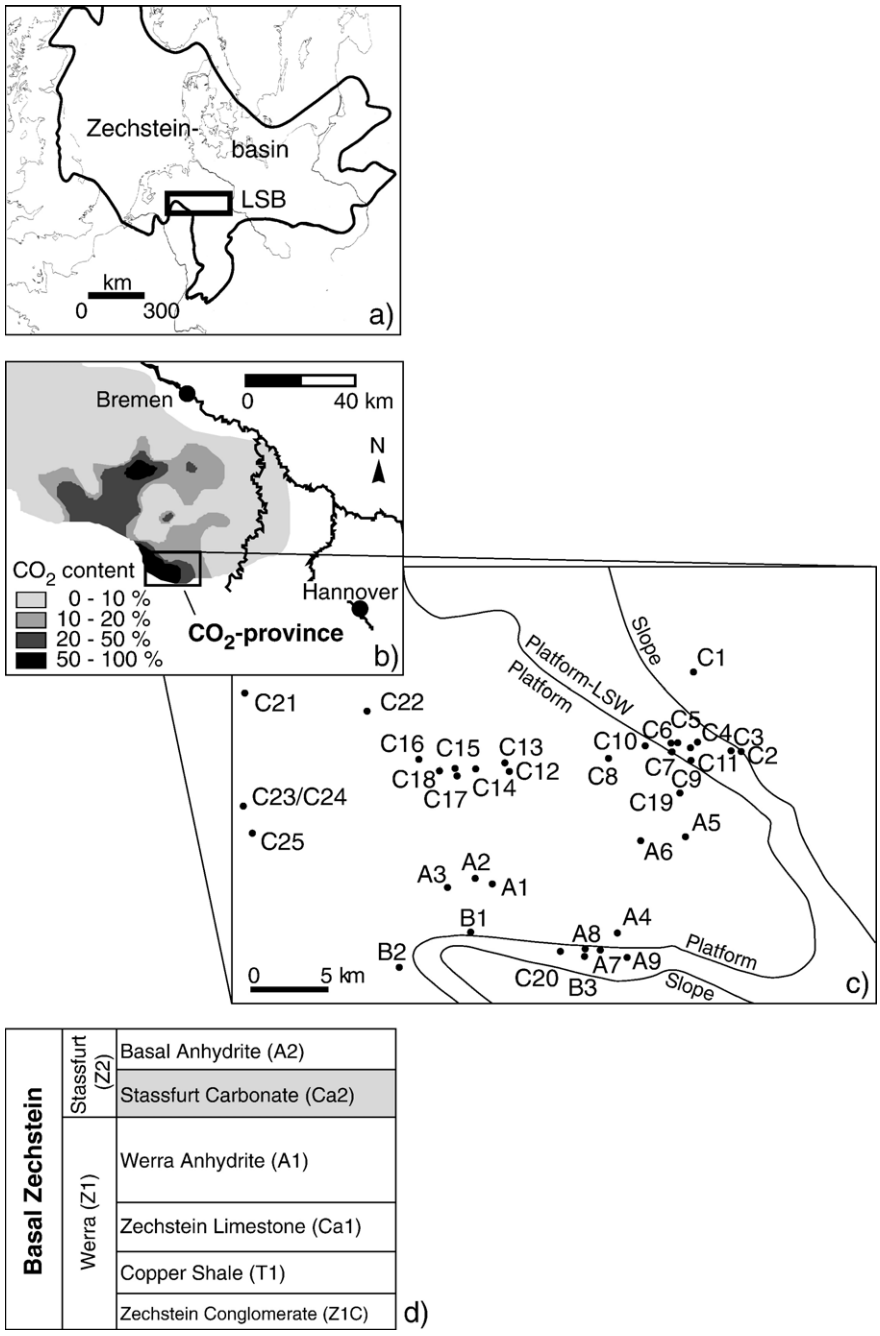

Fig. 1. (a) The Lower Saxony Basin (LSB) located in the southern part of the Zechstein Basin, NW Germany (modified after Füchtbauer and Peryt, 1980). (b) CO_2-gas concentration map of the Lower Saxony Basin (modified after Lokhorst, 1998). (c) Ca2 sourgas field "Wiehengebirgsvorland" with sediment and gas sampling sites (see Table 1A in Appendix and Table 4; LSW = "lowstand wedge"). (d) Stratigraphy of the Basal Zechstein (modified after Strohmenger et al., 1996). The Stassfurt Carbonate (Ca2) layer is marked in grey.

Reservoir quality is a result of both, primary facies and porosity and later diagenetic alteration of porosity and permeability. The Ca2 carbonates have been subjected to multiple diagenetic events that have occurred at different post-depositional times. The present reservoir quality is controlled by five major diagenetic events: (1) meteoric leaching, (2) dolomitisation, (3) displacive and replacive anhydritisation, (4) dedolomitisation (calcitisation) and (5) halite cementation (Strohmenger et al., 1996, 1998).

The Ca2 is typically a fair to good reservoir where it is dolomite. Calcitisation of the Ca2 causes poor to non-

reservoir rocks. The diagenetic history of the Ca2 can be subdivided into early (shallow-burial) and late (deep-burial) diagenetic events. Only halite precipitation cannot be linked unequivocally to either early or late diagenesis. The shallow-water carbonates of the Ca2 platform show predominantly primary interparticle and early diagenetic intraparticle, moldic and vuggy porosities due to meteoric leaching. Previous geochemical studies on Ca2 dolomites (Peryt and Magaritz, 1990; Below, 1992) show that dolomitisation of the shallow-subtidal to supratidal carbonates took place by penecontemporaneous sabkha dolomitisation as well as predominantly mixing-water dolomitisation. The latter was favoured by intra-Ca2 relative sea-level fluctuations (Strohmenger et al., 1996). Ensuing dedolomitisation either destroyed porosity or created additional vuggy porosity as a result of dolomite leaching (Clark, 1980). Strontium isotope analyses suggest that calcitisation fluids derived from the gypsum-to-anhydrite transformation (de-watering) of finely laminated A1 gypsum deposits due to compaction. These fluids presumably caused calcitisation of Ca2 slope dolomites along fault and fracture systems (Love and Strohmenger, 1994). Reservoir quality of the Ca2 carbonates seems thus strongly related to early diagenetic, shallow-burial conditions (less than 500 m) during Late Permian time (Strohmenger et al., 1998).

As mentioned above, the "Wiehengebirgsvorland" area underwent several phases of extensional and compressional tectonics. As a consequence the Basal Zechstein as a part of the pre-salt basement was intensely faulted and fractured. Most likely the Ca2-rock fractures have been cemented during these later stages of deep-burial (Rockenbauch, EMPG, Hannover, personal communication; Strohmenger et al., 1998) and are thus an excellent subject for the present isotope studies. Altogether the drill-sites of the area provide about 520 m of Ca2 carbonate sediment cores and numerous natural gas analyses as basis for these investigations.

1.3. Gas content

The Ca2 reservoir rocks of the gas fields in the central part of the LSB show a large variety with respect to natural gas composition (Gerling et al., 1999). In the Ca2 carbonate, H_2S adds to the non-hydrocarbon components CO_2 and N_2. Even within one reservoir, the individual structural blocks display different natural gas compositions. Thus the amount of CO_2 in the sourgas field of the southern "Wiehengebirgsvorland" varies significantly over short lateral distances: three out of twelve gas-bearing wells show an extremely high amount of CO_2 from 74% up to 91% (Rockenbauch, EMPG, Hannover, personal communication). The complex gas situation described above is the result of the burial history and structural evolution of the LSB. In its central and southern part areas of high thermal maturation (vitrinite reflectance values up to 6% Rr) occur (Düppenbecker and Welte, 1989; Marshallsea, 1995; Pagnier et al., 2003; Drozdzewski et al., 2003) which were previously explained as being caused by magmatic intrusions of Upper Cretaceous age that affected the sedimentary fill of the LSB (Stahl, 1971; Büchner, 1986; Buntebarth, 1985; Deutloff et al., 1980; Rullkötter et al., 1988). Recent investigations, however, involving apatite fission track analysis (AFTA), organic geochemistry, backstripping and structural restoration as well as numerical thermal modeling, indicate that maturation may be closely related to deep burial (Schmitz and Wenzlow, 1990; Senglaub et al., in press) of the individual structures of the LSB along major tectonic faults (Petmecky et al., 1999). As a result of the thermal maturation during burial of the LSB, CO_2 and N_2 were generated (Littke et al., 1995). However, the migration process with time through the overburden sedimentary sequence and the selective accumulation of individual non-hydrocarbon components is not yet fully understood. In addition, the possibility of in-situ generation of H_2S and CO_2 by thermochemical sulfate reduction (TSR) within the Zechstein anhydrites and carbonates (Steinhoff, 1988; Nöth and Steinhoff, 1995) complicates the non-hydrocarbon system further. A reliable prediction of the reservoir gas characteristics and here in particular the non-hydrocarbon components such as CO_2 is dependent on the understanding and quantification of all possible sources of CO_2.

2. Methods

2.1. Grey scale imaging

Digital images were taken from the planar, dry surface of slabbed Ca2 cores. In total, photographs of 140 m of cores from CO_2-rich sites and of about 300 m of cores from CH_4-rich sites were taken. The photos were analysed by quantifying the frequencies of grey tone pixels between black and white (grey scale histogram between 0 and 255) with the image area processing and analysing software package ImageJ. Grey tones representing authigenic fracture and concretion cementing minerals were calibrated and range between grey scale numbers 180 and 230. The amount of these fillings (given in %) is calculated by the ratio of bright pixel quantity (180–230) and the total pixel number determined. The error of this method (3%) is mainly con-

trolled by the determination of the lower limit of grey scale units represented by authigenic minerals (±10).

2.2. Sampling of rock cores

Twelve Ca2 drill cores (three CO_2-rich, nine CH_4-rich) from the "Wiehengebirgsvorland" area (Fig. 1c; Table 1A in Appendix) were made available by the oil companies ExxonMobil and Wintershall for sampling diagenetic mineral occurrences within the rock matrix. Although there is normally a range of fracture sizes from micro to large in any one set (e.g., Gale et al., 2004 and references therein) we concentrated on sampling authigenic minerals by macroscopic evidence only. Typical diagenetic precipitations occur as nodules (concretions; Plate 1a), small (up to millimeter-wide and tenths of centimeter long) mineral-filled cracks (Plate 1b,d) and large (up to 2 cm wide with unknown length) cemented fractures (Plate 1c,e). Bulk samples (~1–400 mg) of the different authigenic minerals were drilled with a micro-drilling device (Proxxon-Carbide drill, 1 mm diameter). All together a total number of 396 samples were collected and analysed for mineralogical and stable isotope composition of authigenic carbonate minerals.

2.3. Mineralogical analyses

Mineral compositions of the authigenic precipitations were determined by X-ray diffraction measurements

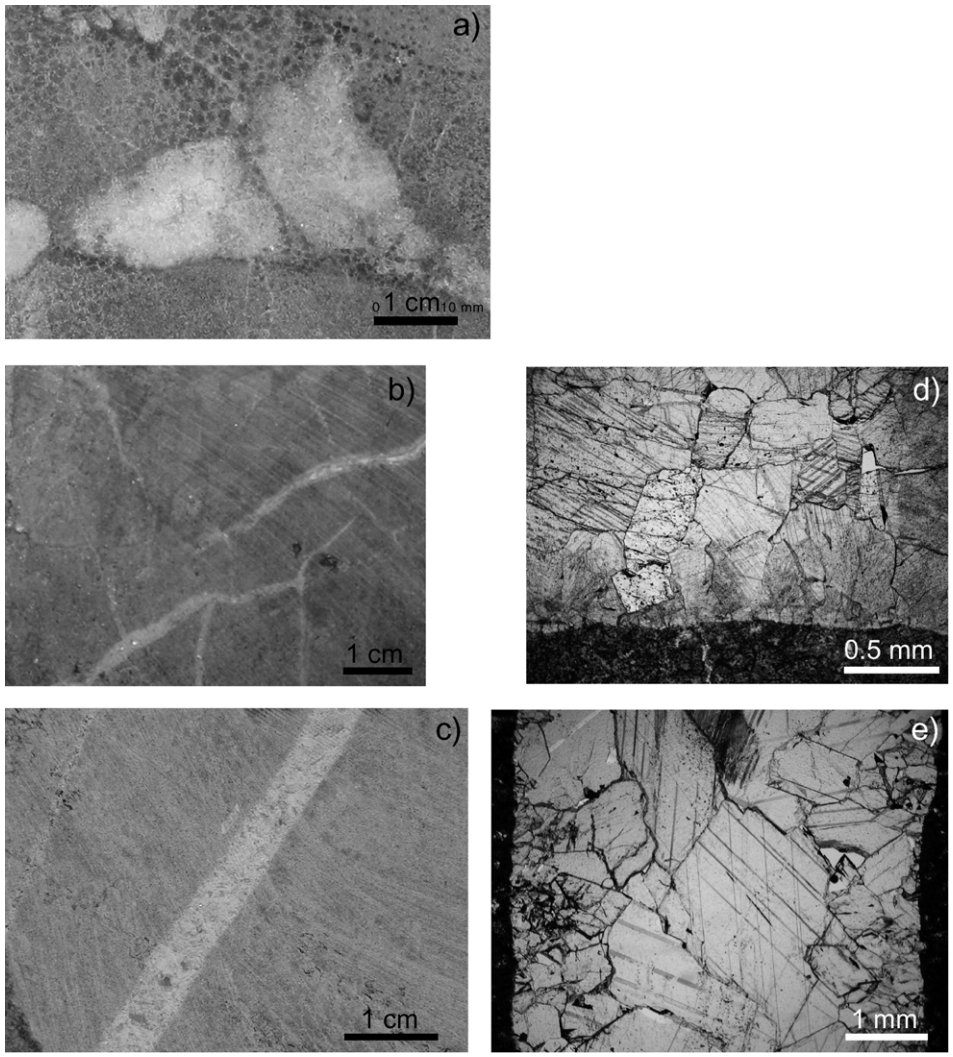

Plate 1. Photographs of authigenic calcite mineralisations observed in the Ca2 rocks. (a) Concretions in sample A7-2a, (b) cracks in sample A4-3, (c) fracture in sample A8-24b, (d) thin section of a crack in sample A7-14a, (e) thin section of a fracture in sample A8-24b; note the crystal coarsening towards the center of the fracture.

(PW 1710/Philips, Cu Kα, 0.02°/s) of bulk samples and by quantifying major peaks of specified minerals in the diffraction patterns. The detection limit for these minerals is approximately 3% (relative mineral concentration).

2.4. Stable isotope analyses

Carbon and oxygen isotope analyses were carried out on both bulk samples and samples from "isotope profiles" (drill diameter 0.2 mm) drilled across selected fractures, cracks and concretions in order to study possible internal variations of the structures (Table 1A in Appendix).

CO_2 of monomineralic calcite and dolomite samples was liberated through reaction with 100% phosphoric acid at 73 °C in an online Carbo-Kiel carbonate preparation line. Calcite/dolomite mixtures were degassed in reaction steps according to Walters et al. (1972). Carbon and oxygen isotope ratios of CO_2 were measured with a MAT 251 IR-MS. The isotope values are reported in the common δ-notation relative V-PDB standard. The standard deviation was about $\pm 0.06‰$ for carbon and $\pm 0.1‰$ for oxygen isotope measurements based on replicate analyses of a standard.

2.5. Radiogenic nuclides

For Sr, Pb isotopic characterisation and isotopic dating we sampled an approx. 3 cm wide mineralised zone (sample A3-6a). The mineralisation is composed mainly of coarse-grained (recrystallised, centimeter-sized) calcite and sphalerite, with minor galena and pyrite. In the immediate vicinity of the mineralisation, the carbonate wallrock is impregnated with pyrite and locally shows small calcite veinlets. Rb/Sr analyses of wallrock material, calcite and sphalerite as well as U/Pb analyses of calcite and galena (Tables 1 and 2) were carried out at the GeoForschungsZentrum Potsdam, following standard procedures (Rb/Sr: Glodny et al., 2002; U/Pb: Romer, 2001).

2.6. Rare earth (REE) and trace elements

Ten authigenic carbonate samples (10–60 mg sample weight) from fractures and cracks were analysed for rare earth and trace element composition by ICP-MS after decomposition with ultrapure subboiled 3 N HNO_3 (Table 3). Precision of the results as determined from replicate analyses was better than 1% RSD for all elements except Yb, Lu (<5% RSD). Accuracy was controlled by analysing international rock standards as unknowns (see Garbe-Schönberg, 1993, for details of analytical procedures).

3. Results and discussion

3.1. Authigenic mineral occurrences

Previous petrographical studies of Ca2 carbonate rocks revealed various modes of diagenetic mineral occurrences (Below, 1992; Strohmenger et al., 1996 and literature cited therein). Similarly, the 12 Ca2 rock cores investigated during this study were found to contain variable amounts and types of authigenic minerals.

Based on XRD-analyses the diagenetic mineral assemblage of the CO_2-rich sites comprises mainly anhydrite (concretionary or crack-filling) and mixtures of calcite plus anhydrite or dolomite. In contrast, the authigenic minerals at CH_4-rich drill sites are dominated by calcite. The reason for this variation in diagenetic mineral contents of CH_4- and CO_2-rich drill sites is unclear. However, obvious differences in the ages (here based on pure petrographic observations) of the mineralisations probably reflect variations in pore water composition with time (Love and Strohmenger, 1994). A detailed discussion of the variable contents and conditions of authigenic mineral formation within Ca2 rocks is beyond the scope of this paper. In the present work the diagenetic carbonate formation is discussed by relating their isotope compositions to the different modes of carbonate occurrence.

Table 1
Rb/Sr analytical data of sample A3−6a

Analysis no.	Material	Rb [ppm]	Sr [ppm]	$^{87}Rb/^{86}Sr$	$\pm 2\sigma$ [%]	$^{87}Sr/^{86}Sr$	$^{87}Sr/^{86}Sr$ $2\sigma_m$ [%]
PS1061	ZnS I	0.17	0.56	0.866	2.5	0.710188	0.0082
PS1055	ZnS II	0.19	0.61	0.874	2.5	0.710474	0.0038
PS1059	calcite I	0.03	131	0.001	15	0.709561	0.0012
PS1051	calcite II	0.01	230	0.000	–	0.709151	0.0012
PS1143	wallrock 1	0.30	46.7	0.019	2.5	0.708246	0.0012
PS1144	wallrock 2	0.24	50.4	0.014	2.5	0.708362	0.0014

ZnS and calcite samples: fragments of single crystals of mineralisation material. Wallrock samples were cut at 1–2 cm distance from the vein mineralisation.

Table 2
U/Pb analytical results of sample A3−6a

Analysis no.	Material[a]	Weight (mg)	Concentrations		Measured[a]		
			U (ppm)	Pb_{tot} (ppm)	$^{206}Pb/^{204}Pb$	$^{208}Pb/^{206}Pb$	$^{207}Pb/^{206}Pb$
PbS1	galena	~0.001	–	–	18.442	2.0885	0.84803
1065	calcite 1	1.69	0.0099	31.40	18.431	2.0862	0.84745
1066	calcite 2	1.73	0.0060	16.84	18.427	2.0876	0.84782

Analysis no.	Atomic ratios[b]	
	$^{204}Pb/^{238}U$	$\pm 2\sigma$ (%)
PbS1	–	–
1065	50.2	6.06
1066	44.2	9.86

Lead isotope composition analysed on a Finnigan MAT 262 multicollector mass spectrometer on single Re−filaments at 1220–1260 °C using Faraday collectors. Element concentrations and U/Pb isotopic ratios of calcite were determined with a $^{205}Pb/^{235}U$ mixed tracer. Two sigma uncertainties in $^{206}Pb/^{204}Pb$ and $^{208}Pb/^{206}Pb$ ratios are <0.1%; uncertainties in $^{207}Pb/^{206}$ Pb ratios are <0.06%.

[a] Corrected for fractionation (0.1%/a.m.u.) and common lead in spike.

[b] Corrected for fractionation and spike, laboratory Pb blank of 15 pg and 4 pg U.

Table 3
Rare earth element and trace element composition (in ppm) of carbonate from fractures and cracks in Ca2 host rock

	A8−23a/II	A8−21a/II	A3−2a	A4−2b	A5−2b	B3−23	B3−70	B3−71	B3−72	B1−41a
Li	0.274	0.204	0.582	0.632	0.538	0.635	0.677	0.776	0.734	4.16
V	0.624	0.445	0.152	0.551	0.096	0.105	2.093	2.413	0.910	0.145
Cr	0.320	0.292	1.76	0.463	0.436	0.551	0.524	0.455	0.249	0.616
Cu	0.550	0.747	26.3	4.91	1.83	1.34	1.10	0.56	0.40	1.25
Zn	4.00	2.612	28.4	44.6	5.880	9.582	4.183	6.954	5.880	13.598
Ga	0.099	0.074	0.174	0.116	0.082	0.019	0.025	0.018	0.016	0.020
Rb	0.201	0.163	0.338	0.409	0.605	0.347	0.341	0.241	0.212	0.384
Sr	290	129	115	303	124	348	432	127	152	161
Y	0.261	0.283	0.598	4.986	0.481	0.101	2.711	0.454	0.429	0.100
Mo	0.025	0.013	0.352	0.050	0.021	0.020	0.022	0.102	0.006	0.300
Sn	0.013	0.008	0.271	0.087	6.82	0.044	0.026	0.101	0.020	0.017
Sb	0.026	0.013	0.110	0.033	0.048	0.025	0.041	0.053	0.014	0.080
Cs	0.017	0.011	0.022	0.028	0.027	0.029	0.037	0.021	0.023	0.127
Ba	453	276	150	28.7	116	7.15	45.5	5.26	1.21	57.5
W	0.051	0.024	0.066	0.038	0.033	0.031	0.032	0.024	0.009	0.032
Tl	<0.005	<0.005	0.432	<0.005	<0.005	0.005	0.005	0.045	0.008	0.019
Pb	2.61	3.53	4.77	0.815	12.9	3.41	0.559	2.98	0.537	1.90
Bi	0.006	<0.005	0.017	0.019	0.036	<0.005	0.005	<0.005	<0.005	0.010
Th	<0.005	<0.005	0.027	0.017	0.009	<0.005	0.009	0.109	0.005	0.015
U	<0.005	0.006	0.028	0.015	0.017	0.018	0.096	0.145	0.057	0.917
La	0.072	0.062	0.072	0.249	0.197	0.087	0.285	0.493	0.459	0.056
Ce	0.211	0.172	0.321	1.24	0.631	0.296	1.26	1.19	1.16	0.153
Pr	0.023	0.017	0.036	0.248	0.062	0.022	0.194	0.147	0.150	0.014
Nd	0.096	0.071	0.186	1.52	0.251	0.093	0.851	0.546	0.561	0.058
Sm	0.028	0.021	0.093	0.791	0.058	0.017	0.274	0.113	0.117	0.014
Eu	<0.1	<0.1	<0.1	0.211	<0.1	<0.1	<0.1	<0.1	<0.1	<0.1
Gd	0.030	0.024	0.141	0.935	0.055	0.013	0.254	0.094	0.085	0.013
Tb	0.004	0.004	0.018	0.148	0.008	0.002	0.056	0.014	0.013	<0.005
Dy	0.025	0.028	0.096	0.849	0.050	0.011	0.391	0.079	0.071	0.012
Ho	0.005	0.006	0.017	0.149	0.010	<0.005	0.079	0.014	0.014	<0.005
Er	0.016	0.021	0.046	0.398	0.030	0.006	0.236	0.041	0.039	0.008
Tm	<0.005	<0.005	0.006	0.051	0.004	<0.005	0.035	0.005	0.005	<0.005
Yb	0.013	0.021	0.035	0.288	0.022	0.005	0.164	0.033	0.035	0.008
Lu	<0.005	<0.005	0.005	0.035	<0.005	<0.005	0.023	0.005	0.005	<0.005

Within the Ca2 rocks different mineral generations were observed. Authigenic minerals in the Ca2 rocks occur as early diagenetic mineral formation in soft or semi-consolidated sediments, e.g., sediment-embedded, roundish concretions (Plate 1a) or small, often lens-shaped cracks indicating sediment contraction (Plate 1b, exhibiting mosaic crystal structure, Plate 1d). This early diagenetic mineral precipitation probably occurred under shallow (soft) sediment cover at times when the pore water was locally oversaturated. Causes for early local carbonate oversaturation within sediments could have been mineral dissolution and subsequent re-precipitation processes (Bathurst, 1976; Morse and Mackenzie, 1990), and/or an increase in alkalinity due to (local) metabolic reactions (Claypool and Kaplan, 1974; Irwin et al., 1977; Pisciotto and Mahoney, 1981).

In contrast, fractures formed in solid Ca2 rocks by tectonic events probably under deeper burial (Strohmenger et al., 1996, 1998). Accordingly, we observed large fracture systems sharply cutting the host rocks (Fig. 2; Plate 1c). 3D-orientations of these fracture systems within the methane-rich rock cores were manifold and structure geological investigations were not performed. In the study area these fractures are usually cemented by mosaic crystals of authigenic calcite. We often observed crystal coarsening towards the center of the fracture (Plate 1e). This could be related to variable carbonate (over-) saturation conditions. Alternatively diagenetic crystal enlargement could be responsible

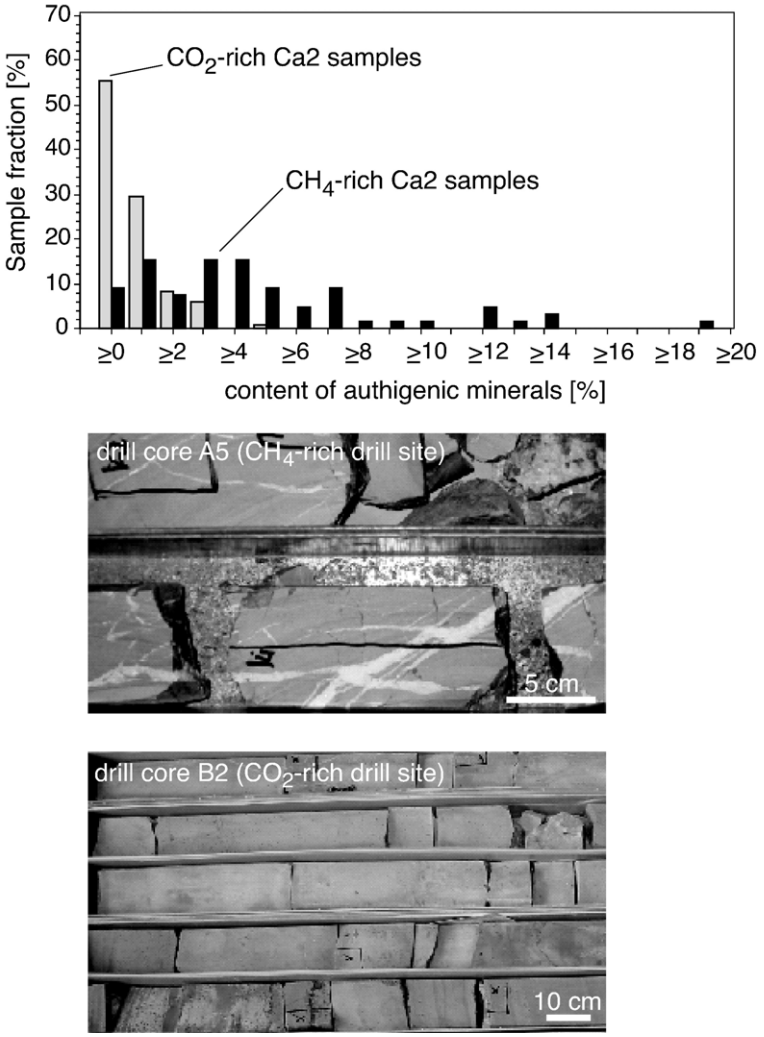

Fig. 2. Frequency distribution patterns in CO_2- and CH_4-rich drill sites estimated by grey scale/pixel analysis of diagenetic mineral content within the investigated Ca2 rock cores. The analysis is based on photographs taken from about 300 m of slabbed cores from CH_4-rich sites (e.g., drill core A5) and from 140 m of slabbed cores from CO_2-rich sites (e.g. drill core B2).

(Botz, 1979). This fracture-filling calcite most likely precipitated due to disturbances of the carbonate equilibrium following CO_2 degassing induced by tectonic pressure release which also caused the rock fractures. The origin of small (Plate 1b,d), sometimes micro-sized cracks is much more obscure. However, those cracks may have formed as a result of early changes in sediment density (e.g., sediment volume) caused by sediment dewatering (for instance during gypsum-anhydrite transformation) and/or dolomitisation/re-calcitisation processes. Alternatively, they could also have formed during deep burial related processes induced by tectonics.

Major authigenic minerals within the Ca2 rocks, such as calcite, dolomite and anhydrite, are light-coloured (in contrast to the host rock) and hence, the relative quantities of authigenic minerals in the sediments could be estimated by grey scale/pixel analysis (cf. Section 2.1). Such semi-quantitative estimates of the diagenetic mineral content for the Ca2 carbonate rocks were made from core slabs (Fig. 2). The CH_4-rich drill sites contain a significantly higher abundance of authigenic minerals. This difference reflects that, besides concretions and cracks which are present in all 12 cores, only the rocks of the CH_4-rich sites contain abundant fracture systems. Such fracture fillings (up to 2 cm wide) were not observed in the carbonate rocks from the CO_2-rich drill sites. Considering the sometimes close vicinity (a few kilometers only) of CH_4- and CO_2-rich drill sites (i.e., A8 and B3 in Fig. 1c), these differences suggest that the local tectonic stress field was variable over very short distances. Hence tectonics did not only control local deformations of Ca2 carbonate rocks but also the gas content of the reservoir rocks.

3.2. Radiogenic nuclides

In order to understand the relationship between time(s) of tectonic movements and gas content/compositions within the Ca2 reservoir rocks we tried to collect information on the absolute age of diagenetic mineral occurrences. $^{234}U/^{230}Th$ equilibria were found for various diagenetic carbonate samples which clearly indicated absolute ages of >300.000 years for the fracture calcite (IFM-Geomar, Kiel, personal communication). Hence analyses of radioactive decay systems with longer half-lives (Rb/Sr, U/Pb) were performed.

3.2.1. Rb/Sr data

Rb/Sr analysis of mineralisation and wall rock material revealed Sr-isotopic disequilibria (Table 1, Fig. 3). Consequently, an attempt to date the mineralisation event using sphalerite (e.g., Walshaw and Menuge, 1998) did not result in a well-defined isochron age. Instead, different Sr isotopic compositions in the two analysed calcite fragments (subsamples in Table 1) indicate Sr-isotopic variability of the mineralising fluids. The isotopic data only support a rough age estimate: the paragenetic relationship between calcite and sphalerite justifies calculation of an apparent *maximum* mineralisation age of 106 Ma using the data for the least radiogenic calcite and the most radiogenic sphalerite. However, confidence of this calculated age is limited as the Sr-istopic variance of the mineralising fluids may have been considerably higher than the variance documented in our four-vein material analyses. From the isotopic data alone, the age of the mineralisation-related tectonic event is thus only loosely constrained to Cretaceous-Paleogene times. The geological framework, in combination with our data, points to a late Early Cretaceous or early Late Cretaceous age for the vein fracture system (see discussion below).

The Rb/Sr data further reveal long-distance advection of the mineralising fluids. Vein wallrock ($^{87}Sr/^{86}Sr$: 0.70824–0.70836) shows significantly lower $^{87}Sr/^{86}Sr$ ratios than vein calcite ($^{87}Sr/^{86}Sr$: 0.70915–0.70956), implying disequilibrium between vein and wallrock material. The vein-hosting Ca2 carbonate is, in the same way as the basal and overlying anhydrite units, part of a marine succession precipitated from seawater with Sr isotopic compositions as low as 0.7067–0.7071 (Kramm and Wedepohl, 1991; Veizer et al., 1999). With $^{87}Sr/^{86}Sr$ values in between Late Permian seawater and vein material, the wallrock samples document progressive Sr isotope exchange between advected mineralising fluids and wallrock, which implies that the original $^{87}Sr/^{86}Sr$ ratios of the mineralising fluids were even higher than the calcite-derived maximum values of 0.70956. Such a signature is indicative for fluids from the regional pre-Late-Permian basement which were, most probably by tectonic pumping during the Upper Cretaceous inversion tectonics, introduced into the Ca2 carbonates along deep-reaching fracture systems.

3.2.2. U/Pb and Pb/Pb data

U/Pb analyses of diagenetic calcite and Pb/Pb analysis of associated galena revealed virtual absence of U from calcite, and identical Pb-isotopic signatures for calcite and galena (Table 2). The measured Pb isotopic signatures (e.g., $^{206}Pb/^{204}Pb = 18.43$) are slightly more radiogenic than those determined for the regional Basal-

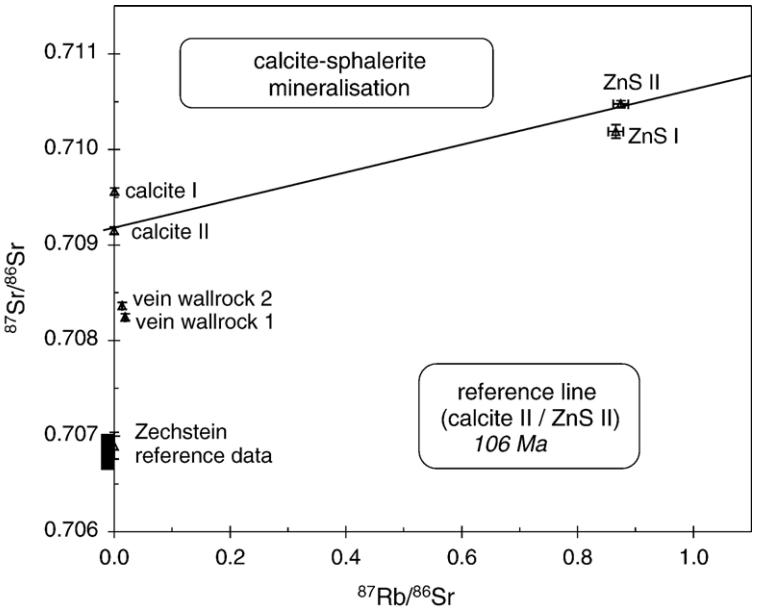

Fig. 3. Rb/Sr data of Ca2 wallrock material, calcite and sphalerite (sample A3-6a). Zechstein reference data (Werra-, Stassfurt- and Leine cycles) is from Kramm and Wedepohl (1991).

Zechstein 'Kupferschiefer' in the Lower Saxony Basin ($^{206}Pb/^{204}Pb$: 18.25–18.28, samples 7 and 8 in Wedepohl et al., 1978). We hypothesise that the Pb associated with diagenetic calcite may represent a mixture between Pb mobilised in Mesozoic–Cenozoic times from the pre-Zechstein basement, and Pb remobilised from the Pb-rich Kupferschiefer bed, down-sequence from the Ca2 carbonates. Such a scenario is well compatible with the Cretaceous-Paleogene large-scale fluid mobilisation system inferred from the Rb/Sr data.

3.3. Authigenic carbonate formation—evidence from REE and trace elements

Systematically changing chemical properties across the series of rare earth elements (REE) make them useful as geochemical tracers for fluid origin, e.g., sea water vs. freshwater water (Zhang and Nozaki, 1998; DeBaar et al., 1985) or hydrothermal sources (Douville et al., 1999) and diagenetic processes (Haley et al., 2004). Thus, variation of REE distributions of fracture carbonates may indicate the changing pore water regimes of the Ca2 rocks during their formation.

Generally, concentrations of all analysed trace elements in the carbonates are very low in the sub-ppm range, only Sr (115–432 ppm), Ba (1–453 ppm), Cu (0.4–26 ppm), Zn (2.6–45 ppm) and Pb (0.5–13 ppm) reach higher concentrations (Table 3). Admixture of a silicate mineral component is low as illustrated by low Ga, Rb, Cs and very little residue after sample dissolution.

After normalisation to average shale (PAAS, Taylor and McLennan, 1985) REE_N in samples from marine environments display a smooth pattern with or without continuous enrichments and depletions of REE subgroups, and discrete anomalies for single REE. Open ocean seawater typically displays a pattern with continuously increasing concentrations towards the heavy REE (HREE, i.e., Dy to Lu, Fig. 4, Group A). This pattern results from the higher stability constants of dissolved carbonate complexes of trivalent HREE and preferential removal of light REE (LREE, La to Nd) by particle scavenging (Bau et al., 1995; Elderfield and Graeves, 1982). Three distinct anomalies characterise seawater further: (i) Ce is selectively removed from seawater by oxidative and irreversible scavenging of Ce^{IV} on particle surfaces leading to a pronounced negative Ce anomaly; (ii) in contrast to endogenic processes where Y behaves similarly to Ho, and $(Y/Ho)_N$ is ≈ 1, particle scavenging in seawater leads to a relative enrichment of dissolved Y making it more similar to LREE under these conditions, with $(Y/Ho)_N > 1$ (Bau et al., 1995; Nozaki et al., 1997); (iii) as a consequence of the tetrad effect dissolved complexes of Gd have a slightly higher stability than its neighbouring REE leading to a weak positive Gd_N anomaly (e.g., Alibo and Nozaki, 1999). All these features of REE distribution in seawater are mirrored by primary marine carbonates. During early diagenesis, these processes are reversed: degradation of marine particles leads to a release of formerly scavenged,

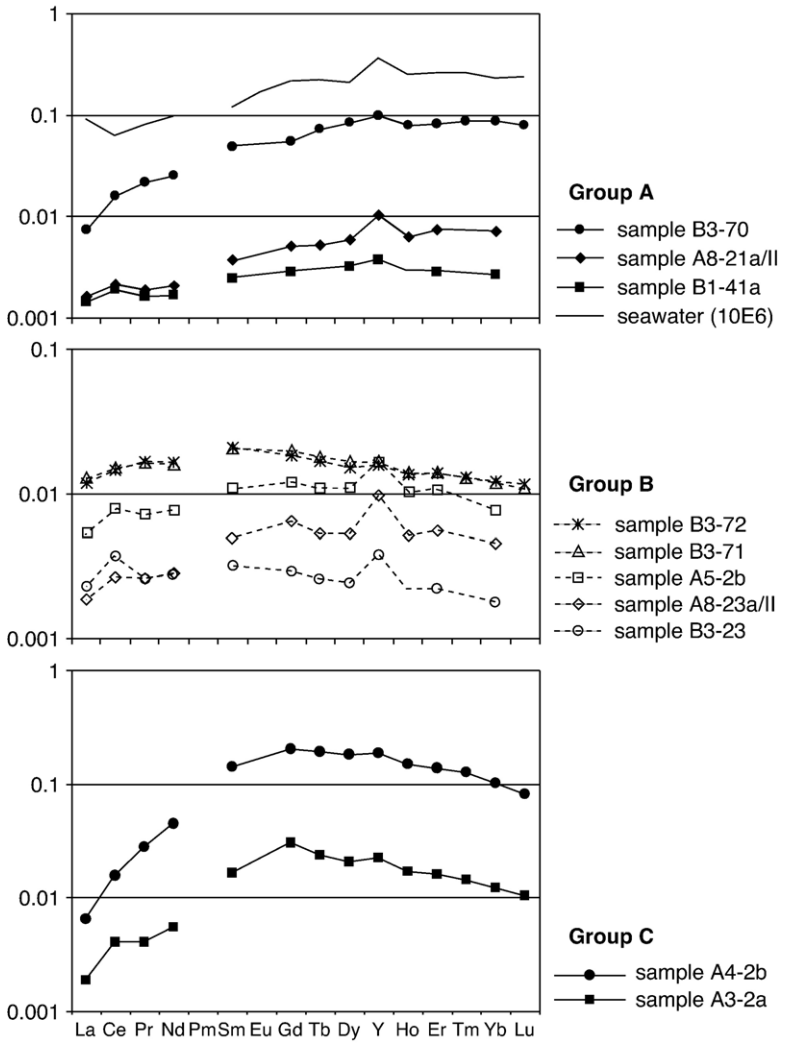

Fig. 4. PAAS-normalised REE pattern for carbonate samples from fractures and cracks in Ca2 host rocks (PAAS, Taylor and Mc Lennan, 1985).

weakly bound REE such that pore water becomes *relatively* enriched in LREE and especially Ce when compared to normal seawater. Progressing diagenesis of carbonates with a certain admixture of clay minerals (which are present in minor amounts in the Ca2 rocks; Botz, 1979) will lead to increasingly shale-like pore water REE. The studied carbonates can now be subdivided into three groups on the basis of their REE_N spectra (Fig. 4):

3.3.1. Group A carbonate

Continuously increasing concentrations towards the HREE with $(La/Sm)_N$ and $(Dy/Lu)_N < 1$, and $(Y/Ho)_N > 1$ is a signature typical for seawater. Cerium, however, displays a weak positive anomaly with $(Ce/Ce^*)_N = 1.1$ indicating that these carbonates precipitated not from a fluid source resembling normal open ocean seawater but from a reducing diagenetic fluid which was relatively enriched in Ce. Hence, the fluid probably was an early diagenetic pore water enriched in Ce after reductive release from degraded marine particles. The three samples in this group display a trend towards *(relatively)* increasing LREE reducing the steepness of the REE pattern. This is accompanied by an increasingly positive Ce anomaly. This may suggest that the carbonates precipitated from different temporal stages of evolving diagenetic fluids (see discussion below).

The carbon isotope values of these fracture and crack carbonates are positive between +1.3‰ (B3-70) and +0.1‰ (A8-21a/II) which supports the idea of a predominating marine carbon source for these carbonates also during late stage diagenesis (see discussion of isotope results below).

3.3.2. Group B carbonate

Two carbonate samples (A8-23a/II and A5-2b) have almost horizontal, shale like HREE pattern with $(Dy/Lu)_N = 1$ but still depleted LREE ($La/Nd_N < 1$) and a positive Ce-anomaly. However, the relative LREE depletion is less pronounced than that of the Group A carbonates. Sample B3-23 leads over to samples B3-71 and B3-72 which are characterised by an enrichment of middle REE_N (MREE, i.e., Sm to Tb) and $(La/Lu)_N = 1$. This trend continues that of Group A samples suggesting that carbonate continuously precipitated from a further evolving late diagenetic fluid, possibly releasing REE from clay and other silicate minerals.

The negative $\delta^{13}C$ values between −2‰ and −2.7‰ are supporting evidence for admixed organic-derived carbon to the normal marine carbon source during late diagenesis of the Ca2 rocks from these drill sites. Samples B3-71 and B3-72 do not show seawater signatures but more or less shale-like LREE and HREE, with an enrichment of MREE.

3.3.3. Group C carbonate

Characteristic feature of the REE_N in carbonate samples from this group is their bell-shaped pattern with high MREE concentrations. The LREE, however, still show the strongly depleted signature of seawater ($La/Sm < 1$). Bell-shaped REE patterns with $(La/Yb)_N < 1$, $(Tb/Yb)_N > 1$ are described from biogenic phosphates and are thought to be the product of secondary alteration with selective removal of HREE (Shield and Webb, 2004). Johannesson and Zhou (1999) describe acid leaching or dissolution of MREE enriched FeMn oxides/hydroxides from sedimentary rocks as a likely source for MREE enrichment in acid lake water. Concentrations of other trace elements are anomalous in these samples (A3-2a, A4-2b), with highest Co, Cu, Zn and Cr, Mo, Sb, Bi, W, Tl and Pb (refer to Table 3). This suite of elements is typically enriched in reduced fluids under an elevated temperature regime, bearing evidence that these fracture and crack carbonates may have been overprinted by, or originated from, hydrothermal fluids. Sample A4-2b is mineralised showing macroscopic pyrite.

3.4. Authigenic carbonate formation—evidence from stable isotopes

3.4.1. Early diagenetic carbonate

Primary marine carbonates form in (or near to) isotope equilibrium with atmospheric CO_2 ($\delta^{13}C = -7‰$; Keeling, 1958; pre-industrial likely near −6.5‰). At 20 °C (an assumed sea surface water temperature) there is a fractionation of about 10‰ between dissolved CO_2 and solid carbonate (Emrich et al., 1970; Romanek et al., 1992) and thus, a $\delta^{13}C$ value near +3‰ is characteristic for marine carbonate that precipitated in equilibrium from modern ocean surface water. Marine carbonates deposited worldwide during Permian time, however, have ^{13}C enrichments of several permil (up to 8‰ based on fossil shell analyses; Veizer et al., 1999). More specifically for Ca2 carbonates $\delta^{13}C_{carbonate}$ values around +7‰ to +8‰ have been observed (Botz, 1979; Magaritz and Schulze, 1980; Clark, 1980; Magaritz et al., 1982).

Explanations for this ^{13}C enrichment in carbonates are biologically mediated redox processes (Veizer et al., 1999). For Permian carbonates Magaritz and Schulze (1980) postulate that a ^{13}C anomaly was caused by deposition of excess ^{12}C-rich organic carbon in ocean basins. Similar mechanism had previously been suggested for different areas by other authors (Garrels and Perry, 1974; Schidlowski et al., 1975; Veizer et al., 1980). In contrast, Clark (1980) concluded bacterial fermentation processes during diagenesis to be responsible for the ^{13}C-enriched Zechstein carbonate sediments.

The stable isotope compositions of authigenic carbonates reflect their different mode of formation and, thus, conclusions about sediment-diagenetic processes can be drawn (Irwin et al., 1977; Pisciotto and Mahoney, 1981; Kelts and McKenzie, 1982).

$\delta^{13}C$ and $\delta^{18}O$ isotope values for all diagenetic carbonate samples (Table 1A in Appendix, Fig. 5) investigated during this study cover a wide range. This indicates changes in the CO_2 source ($\delta^{13}C$) and the formation temperature and/or pore water isotope composition ($\delta^{18}O$) during early to late stage authigenic carbonate formation.

The most positive $\delta^{13}C$ values up to +7.2‰ were found for a large number of early nodular carbonate concretions and also for numerous carbonate precipitations within small cracks. These positive carbon isotope values are within the range of values accepted for Permian carbonates (Magaritz et al., 1981; Magaritz and Schulze, 1980; Botz and Müller, 1987; Veizer et al., 1999). On the other hand the $\delta^{18}O$ values for these authigenic Ca2 carbonates (nodules and cracks) vary between 0‰ and approximately −13.9‰ PDB (Table 1A in Appendix, Fig. 5). There is no direct way to deduce the oxygen isotope composition of the (pore) waters from which the diagenetic minerals precipitated (and/or re-equilibrated with) and, thus the discussion on mineral formation temperatures of the Permian carbonates is problematic. Nevertheless, such negative carbonate oxygen isotope values are often characteristic of

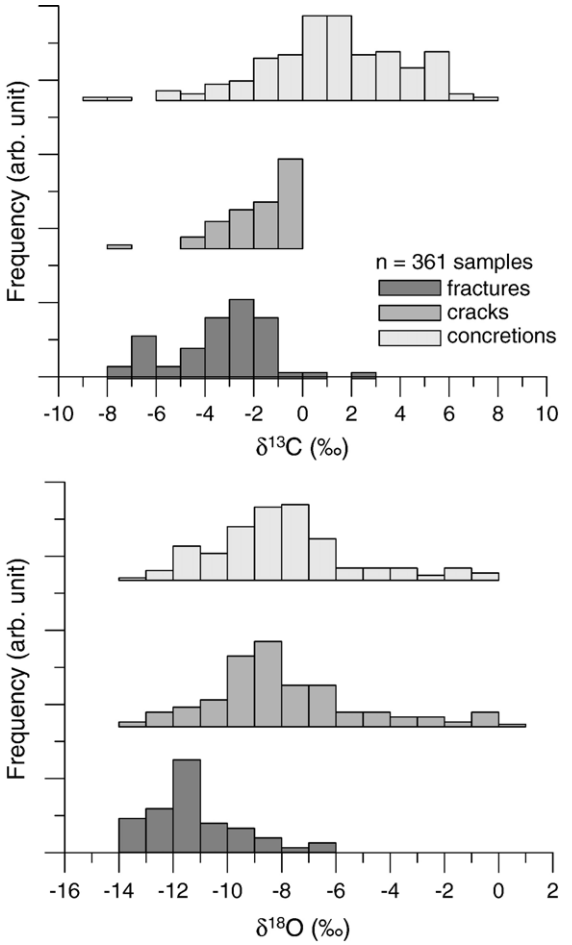

Fig. 5. Results of stable carbon and oxygen isotope investigations of early to late diagenetic carbonate occurrences (concretions, cracks and fractures) within Ca2 reservoir rocks.

fresh water environments and may indicate meteoric diagenesis. Although carbonate rocks from the Ca2 platform facies are subjected to meteoric leaching, carbonate cements related to meteoric diagenesis such as the sparitic cements from drill site Siedenburg Z6 (Botz, 1979) are only rarely found. The carbonate rocks investigated during the present study did not show these indications of meteoric diagenesis and thus, for the rock cores under consideration, a fresh water origin for these carbonate precipitations could not be documented petrographically. Based on isotope analyses of brachiopod shells, Veizer et al. (1986) postulated an oxygen isotope value near 0 ± 1‰ (SMOW) for the Permian seawater. A wider range to more negative oxygen isotope values was published for brachiopods by Veizer et al. (1999). The NW-German Basin represents a separate (semi-enclosed) sub-basin, however, and its waters might have been enriched in ^{18}O ($\delta^{18}O > 0$‰ SMOW) by evaporation. We analysed no fossils in our sediment cores from the NW-German Basin and hence, the isotopic composition of the seawater in this part of the basin during Zechstein time cannot be inferred. The only method to deduce the oxygen isotope composition of the pore waters is to use the oxygen isotope values of the minerals themselves. However, carbonate minerals are subject to recrystallisation and isotopic re-equilibration processes at high temperatures which cause secondary decrease of the ^{18}O content of carbonate minerals that then would indicate high mineral formation temperatures (Veizer and Hoefs, 1976; Morse and Mackenzie, 1990 and literature cited therein). Fine-grained Zechstein dolomites, however, are probably not affected by recrystallisation and re-equilibration (Magaritz and Schulze, 1980). Thus, the most promising way to infer the oxygen isotope composition of the early Ca2 (pore) waters is to study the isotope composition of fine-grained ("non" recrystallised) primary to early diagenetic (Ca2) dolomites. These Ca2 dolomites display $\delta^{18}O$ values between −3‰ and +2‰ PDB (with $\delta^{18}O_{dolomite}$ values up to +5‰ in associated evaporitic anhydrite sediments; Botz and Müller, 1981; Below, 1992; Fig. 6). Formation temperatures between 34 °C and 60 °C using the equation of Northrop and Clayton (1966) can then be calculated for the dolomite precipitation ($\delta^{18}O_{water} = 0$‰ SMOW). This range of temperatures for early diagenetic dolomite formation appears not to be unrealistic (Land, 1980; McKenzie, 1981; Patterson and Kinsman, 1982; Hardie, 1987). If ^{18}O-enriched (approx. 2‰ by evaporation) waters are assumed during dolomite formation the calculated precipitation temperatures for the early dolomite would be slightly higher (~70 °C).

On the other hand, if freshwater contributed to the dolomite precipitation (Below, 1992) or a secondary decrease in the ^{18}O-content of the early formed dolomites due to (minor) re-equilibration with surrounding pore waters at high temperature (Fig. 6) is assumed, the actual formation temperatures of the early diagenetic dolomite would be somewhat lower than the 34–60 °C range calculated above.

On the basis of these results it seems adequate to use a $\delta^{18}O$ value of 0‰ also for the early diagenetic (sea water-derived) pore water in order to calculate the formation temperatures of calcite in concretions and cracks (Table 1A in Appendix). The calculated isotopic formation temperatures of early diagenetic calcite concretions (e.g., those with Permian-related positive $\delta^{13}C$ values; Table 1A in Appendix) are sometimes rather high, up to ~107 °C (O'Neil et al., 1969; sample A1-1). However, the concretions investigated during this study often

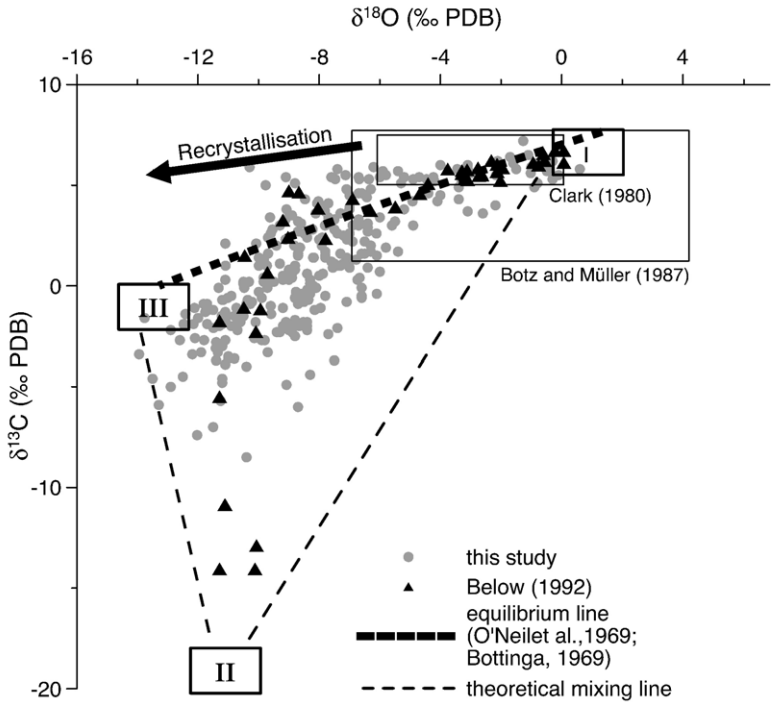

Fig. 6. Stable carbon and oxygen isotope values of diagenetic calcitic cements analysed in this study in comparison with isotope data from Ca2 carbonate investigations from Below (1992), Botz and Müller (1987) and Clark (1980). Temperature-controlled isotope re-equilibrium line (Bottinga, 1969) is calculated with $\delta^{18}O_{water}$ ~0‰ (SMOW) after O'Neil et al. (1969) and $\delta^{13}C_{CO2}$ ~ −4‰. $\delta^{13}C/\delta^{18}O$ compositions of carbonate endmembers are indicated by three fields (e.g., "I" = Permian carbonate. "II" = organic-derived carbonate. "III" = recrystallised Permian carbonate).

show diagenetic crystal enlargement caused by recrystallisation processes. Botz (1979) and Below (1992) have found a correlation between the crystal size of carbonate concretions and their $\delta^{18}O$ values (i.e., large crystals have "light" oxygen isotope values). Thus, secondary isotopic re-equilibration may have influenced the isotopic composition of concretionary calcite (Fig. 6, T-dependent re-equilibration), which indicates high formation temperatures (see also discussion below). Moreover, late diagenetic replacive carbonate growth and/or late internal carbonate cementation within the concretions may also be responsible for their broad range of negative carbon and oxygen isotope values measured (Table 1A in Appendix; Fig. 5; see below).

Very similar to the large range of isotope values measured for the concretions we found also a wide range of carbon and oxygen isotope values for carbonates which precipitated in numerous cracks within the Ca2 rocks (Table 1A in Appendix; Fig. 5). Less variable isotope values were found for detailed profiles across individual cracks indicating usually only minor changes in water conditions (e.g., carbon source and carbonate formation temperatures) during individual crack cementation (Table 1A in Appendix). However, isotope formation temperatures vary between ~17 °C and ~103 °C ($\delta^{18}O_{calcite}$ = − 0.3‰ and −13.5‰; $\delta^{18}O_{H2O}$ = 0‰) for all crack-cementing carbonates. Low temperatures calculated for carbonates with seawater related (Permian) CO_2 carbon isotope values probably indicate the low sediment temperature, which prevailed during cementation of early formed cracks. However, carbonate cementations of various cracks apparently occur up to relatively high temperature (~100 °C). Thus the revealed isotope values most likely represent different carbonate generations (and/or recrystallisation and isotope re-equilibration) during sediment subsidence. The temperature ranges of calcite precipitation within cracks fit approximately the temperatures calculated for early diagenetic dolomitisation.

3.4.2. Late diagenetic carbonate

Negative oxygen isotope values from −6‰ to −13.4‰ PDB were found for late diagenetic fracture calcite with $\delta^{13}C$-values of about +2.3‰ to −7.7‰ PDB. Detailed stable isotope profiles across selected fractures usually show relatively homogenous carbon and oxygen isotope values (Fig. 7; Table 1A in Appendix), indicating carbonate precipitation under constant pore water conditions prevailing in the Ca2 reservoir rocks some time during late diagenesis. The exception

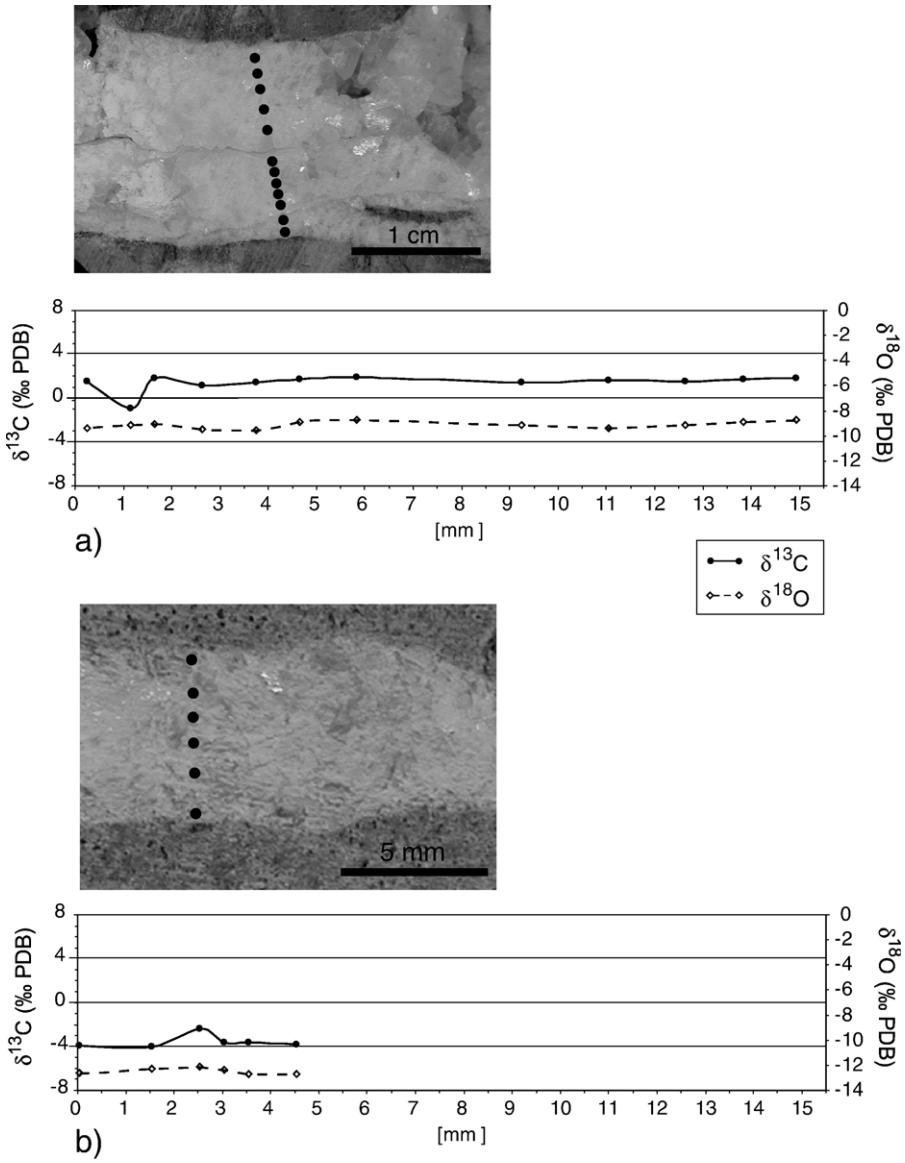

Fig. 7. Detailed carbon and oxygen isotope analyses across selected carbonate-filled fractures in samples (a) A5-2a and (b) A5-2b.

is sample A9-5a (Table 1A in Appendix), which shows an about 10‰ higher δ^{13}C-value for carbonate precipitated in the central part of the fracture compared with the rim zones. This probably reflects carbonate precipitation associated with a change in the carbon source from marine derived HCO_3^- ($\delta^{13}C_{carb.} \sim +2‰$) to a mixed marine/biogenic CO_2 source ($\delta^{13}C_{carb.} \sim -7.5‰$). The reason for this isotopic variation is unknown although dissolution and reprecipitation of primary carbonate within the central part of this late diagenetic fracture is possible. The idea of late diagenetic carbonate redistribution is supported by the negative δ^{18}O-values ($-6‰$ to $-10‰$) indicating high carbonate formation temperature.

The negative δ^{18}O-values reflect carbonate precipitation in solid rocks, probably at greater depth and higher temperatures of up to 102 °C (assuming $\delta^{18}O_{water} = 0‰$; field III in Fig. 6). A similar range of temperatures (75–110 °C) was determined for the formation of fluid inclusions in Ca2 fracture carbonates (Liedmann, 1992). However, isotope studies of interstitial waters showed that with increasing water/rock reactions at high temperatures (causing low isotope fractionation between mineral and water) the ^{18}O content of pore waters may increase by several permil (Fritz and Fontes, 1986). A secondary ^{18}O enrichment of pore water is perhaps supported by the Rb/Sr and U/Pb data of sample A3-6a, which indicates the local

importance of deep-seated fluids influencing the pore water regime of the Ca2 sometime during early to late diagenesis (note that the A3 well is located close to a major distortion system). These fluids could theoretically have a maximum $\delta^{18}O_{water}$ value near +7‰ (end-member value for magmatic water, Truesdell and Hulston, 1980). If the fracture carbonates had formed from ^{18}O-enriched waters (assuming +2‰ to +4‰ SMOW; e.g., possible mixtures of Permian sea water and ^{18}O-enriched fluids) higher formation temperatures (~120–150 °C) are calculated using the most negative $\delta^{18}O$ value for such late diagenetic carbonates.

A temperature/age relationship was modelled using PetroMod software of IES, Aachen. Results for one key well are shown in Fig. 8a and b. For calibration of the models vitrinite reflectance values were available. 1D-modelling of burial and temperature history was performed for a total of 20 wells following established procedures (Poelchau et al., 1997; Yalcin et al., 1997). A detailed 1D- and 2D-basin modelling study for the same area was published by Petmecky et al. (1999). Results obtained here are in principal agreement with those of this earlier study. In Fig. 8a the burial and temperature history for a well in the central part of the study area (see Fig. 1c, well A3) is shown. Well-calibrated models are obtained using a heat flow of 60 mW/m^2 (typical continental crust; Allen and Allen, 1990) for the Cretaceous when deepest burial and highest temperatures were reached. For simplicity, the same heat flow was also applied for the earlier and later times of basin evolution. It should be noted that the same principal evolution of burial and uplift results for all wells in the study area, but that the depth of maximum burial as well as the amount of Late Cretaceous uplift is highly variable (Petmecky et al., 1999).

The resultant maximum temperatures of about 220 °C for the Basal Zechstein were reached during the early Late Cretaceous (Fig. 8a). During the Triassic and Jurassic, temperatures remained below 100–120 °C and were at similar low levels during the Tertiary post-inversion phase.

According to this model and considering the $\delta^{18}O$ values of the carbonate the time of diagenetic mineralisation may be either during later stage of LSB-subsidence (~130 Ma) or during the inversion of the LSB (~70 Ma–80 Ma). The age estimation based on Rb/Sr data, which points to a maximum age of about 106 Ma for the 1–2 cm large crystals cementing open pore spaces from drilling A3 (see above), rather supports the younger age during the inversion phase to be the likely time span of major late diagenetic mineral formation. However, additional information on the absolute ages of mineralisations within single drill cores are needed in order to establish a more detailed relationship between the Ca2 history of subsidence, uplift and/or tectonic movements and related diagenetic mineralisations.

The $\delta^{13}C$ values of the fracture-filling carbonate in Ca2 rocks generally fall in a negative range (down to ~−14‰, Fig. 6). ^{12}C-rich carbon pools within sediments are attributed to different microbial mediated processes of organic matter degradation (e.g., Presley and Kaplan, 1968; Claypool and Kaplan, 1974; Whelan et al., 1978; Sackett et al., 1979). Authigenic carbonates reflect those (bio)geochemical processes. For instance, negative carbon isotope values near −20‰ can be found in anaerobe sediments where the organic matter is oxidized during sulfate reduction (e.g., Chow et al., 1996). Even more negative carbon isotope values (to −70‰) are attributed to CH_4 oxidation (e.g., Hodgson, 1966; Fritz et al., 1971; Roberts and Whelan, 1975; Irwin et al., 1977; Paull et al., 1992). However, the mineral formation temperatures of most fracture carbonates are relatively high and thus, they probably do not represent early diagenetic metabolic reaction zones within the sediment. At high temperatures when bacterial activity ceases thermal decarboxylation reactions and thermochemical sulfate reduction produces ^{12}C-rich CO_2 (Krouse et al., 1988; Machel et al., 1995), which subsequently may be incorporated in authigenic minerals. In any case the negative carbon isotope values of authigenic carbonates within the Ca2 rocks indicate two carbon sources. In addition to the Permian sea water-derived carbon source (field I in Fig. 6) a ^{12}C-enriched carbon source (approximately indicated by field II in Fig. 6) contributed to the overall carbon pool during sediment diagenesis. Isotope data show (Table 1A in Appendix, Fig. 5) that not only the fracture-filling carbonates are influenced by the ^{12}C-rich carbon source. Also numerous carbonate samples from concretions and cracks incorporated CO_2 which derived from organic matter oxidation. This confirms the complex situation of carbonate formation within concretions and cracks over a wide range of conditions during various diagenetic stages of the Ca2 carbonate rocks (see also discussion above).

In Fig. 6 the theoretical mixing lines between field II and fields I and III are shown. Field III represents “high-temperature”, re-equilibrated carbonate without significant contributions of ^{12}C-rich organic-derived CO_2. This “ternary” diagram, which includes most of the diagenetic carbonate samples suggests actual mixing between the three carbonate endmembers. However, some carbonate samples with

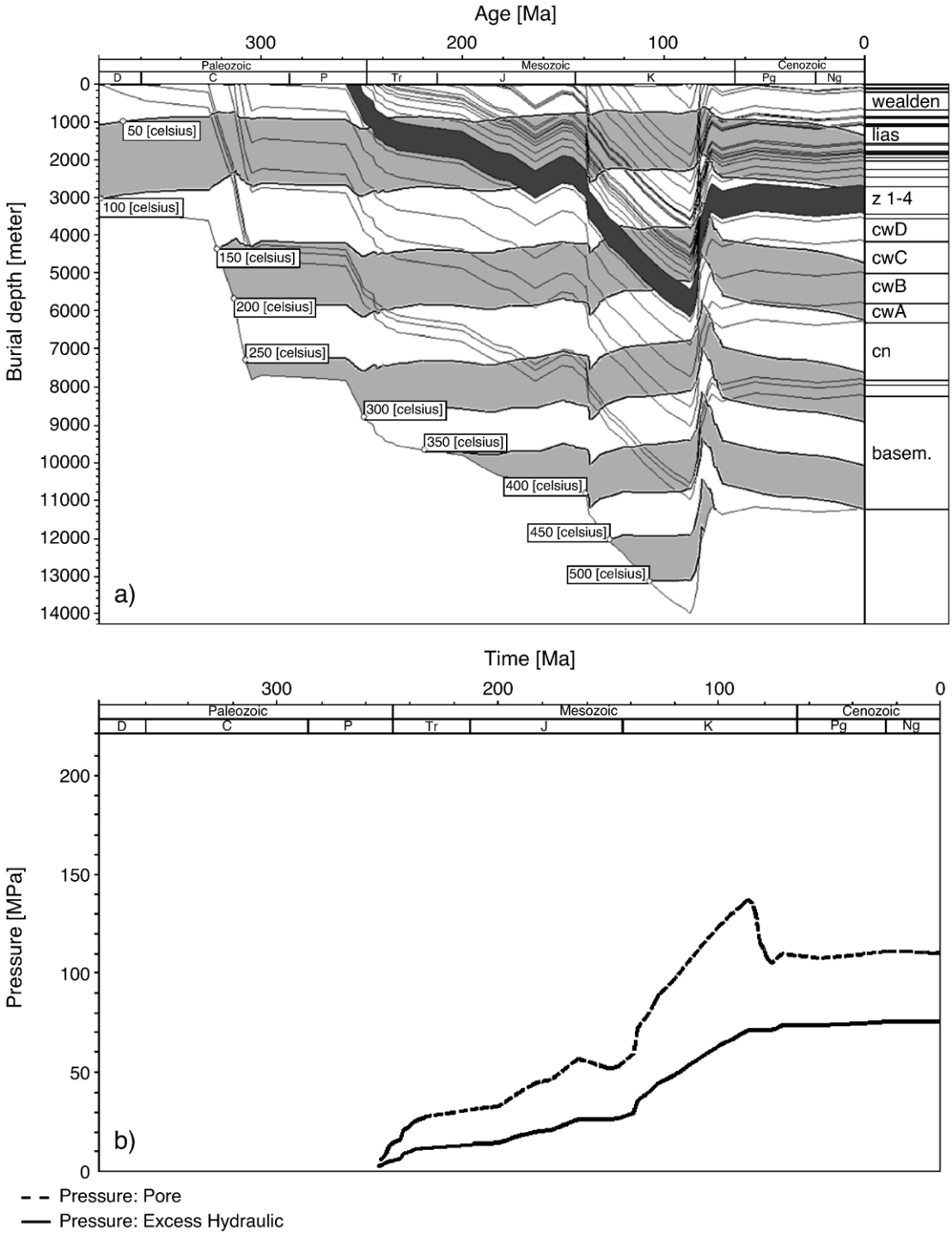

Fig. 8 (a). Burial and temperature history for sedimentary units drilled in well A3. Zechstein layer is marked in dark grey. (b) Pore pressure and overpressure calculated for Basal Zechstein in well A3.

positive $\delta^{13}C$ and negative $\delta^{18}O$ values plot "above" the equilibrium line which cannot be explained by a simple mixing process of these endmembers. These carbonate precipitations in concretions and early-formed cracks may either reflect contributions of ^{13}C-enriched (residual) CO_2 from early (bacterial) methanogenic processes or, alternatively, a freshwater influence during early diagenesis.

Table 4
CO_2 concentrations and $\delta^{13}C_{CO2}$ values of Ca2 reservoir gases in the CO_2-province of the so−called "Wiehengebirgsvorland" (Lower Saxony Basin)

Sample ID	CO_2 (%)	$\delta^{13}C_{CO2}$ (‰ PDB)
A1	20.9	−3.9
A2	17.0	−4.8
A4	20.7	−1.4
A7	10.8	−1.3
A8	10.1	−1.1
C1	8.4	−5.7
C2	9.8	−3.0
C3	10.0	−3.3
C4	10.1	−3.0
C5	9.3	−3.6
C6	9.3	−3.3
C7	9.3	−3.3
C8	9.1	−11.3
C9	9.1	−4.9
C10	9.5	−4.7
C11	9.0	−4.3
C12	9.2	−15.0
C13	9.5	−16.5
C14	10.6	−13.1
C15	8.7	−4.5
C16	42.2	−4.5
C17	28.6	−0.7
C18	28.3	−0.9
C19	8.5	−6.5
C20	78.8	0.4
C21	21.8	−12.4
C22	6.7	−6.6
C23	19.0	−1.3
C24	19.2	−1.6
C25	52.2	−1.0

Data are provided by P. Gerling (BGR, Hannover).

3.5. Origins of CO_2 gas in Ca2 reservoir rocks

The CO_2 contents range between approximately 0% and 90% in the Ca2 reservoir rocks (Lokhorst, 1998). At present the source(s) of the locally high amounts of CO_2 in the so-called CO_2-province of the "Wiehengebirgsvorland" is largely unknown. Available carbon isotope data of authigenic carbonate minerals from Ca2 reservoir rocks suggest a ^{12}C-enriched carbon source must have prevailed in the Ca2 pore water some time during diagenesis. As the fracture carbonates are most likely related to tectonic events (Strohmenger et al., 1996) local pressure release followed by CO_2 degassing processes may have triggered carbonate precipitation within open fractures. Pressure release may have been most pronounced during the Cretaceous phase of deep burial and also during the Tertiary. Pore pressure and overpressure calculation (Fig. 8b) reveal that high overpressures developed during rapid Cretaceous burial. Fluid retention below and within the evaporitic Zechstein units will have been effective and may have caused maintenance of overpressures for long periods of time. According to Fig. 8b the overpressures are completely retained and there is no pressure release during the inversion period and the Tertiary. This fact is, however, influenced by 1D-modelling in which an almost impermeable evaporite layer is assumed; in three dimensional reality, there are usually fluid pathways available which allow pressure release even within an evaporitic series over geological time.

The carbon isotope composition of modern CO_2 occurring within the Ca2 reservoir rocks seems to be related to the CO_2 content within the reservoir gas (Table 4, Gerling, BGR, personal communication). The most positive $\delta^{13}C$ values (Fig. 9) were measured for reservoir gases with high CO_2 contents whereas low CO_2 concentrations are characterised by negative carbon isotope values. This suggests a mixing process between two carbon source endmembers which are represented by field A and B in Fig. 9. The two fields correspond also roughly to the carbon source endmembers assumed for diagenetic carbonate formation. The ^{12}C-rich CO_2 ($\delta^{13}C \sim -20‰$; "A") most likely derived from organic matter degradation. The second "heavy" CO_2 source ($\delta^{13}C \sim 0‰$; "B") was locally admixed to, or replaced, formerly prevailing ^{12}C-enriched CO_2. Variable mixing situations between these two CO_2 endmem-

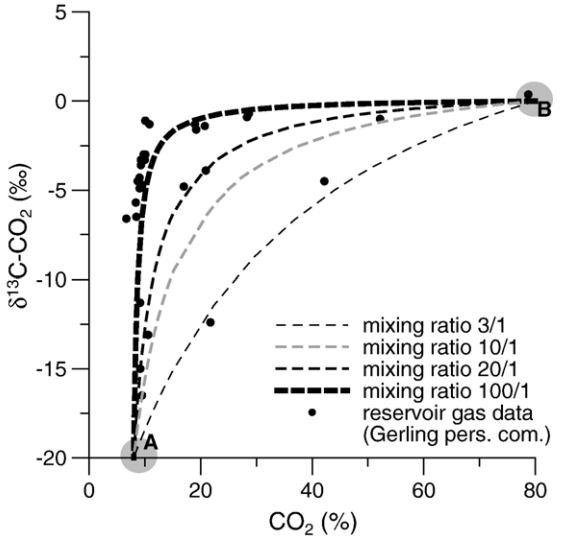

Fig. 9. CO_2 concentration data of reservoir gases sampled in wells of the LSB. Data represent possible mixing situations of fluids from different origins. Endmember "A": low CO_2 concentration of biogenic origin ($\delta^{13}C \sim -20‰$). Endmember "B": high CO_2 concentration from carbonate decomposition ($\delta^{13}C \sim 0‰$). Theoretical mixing curves represent different ratios of CO_2 concentrations of two mixing fluids with $\delta^{13}C$ values for endmember gases "A" and "B", respectively.

bers are indicated in Fig. 9, which probably determine the relationship between concentration and isotope composition of modern CO_2 within the Ca2 reservoir rocks.

The absolute quantities of the CO_2, which derived from these two sources are not known. Based on the gas samples analysed 80% of the total reservoir gas may consist of CO_2 with a positive carbon isotope value near 0‰ (Table 4). Such "heavy" carbon isotope values of CO_2 are only known to be produced during (early) bacterial methanogenesis by CO_2 reduction (Claypool and Kaplan, 1974; Irwin et al., 1977; Whiticar et al., 1986) and from carbonate decomposition processes (Clayton et al., 1990). For the Ca2 rocks carbonate decomposition processes are much more likely (Smith and Ehrenberg, 1989; Cathles and Schoell, 1999, Brown, 1999) as bacterial CH_4 was not found in the reservoir gases and biogeochemical processes are unlikely to occur at high temperatures during late diagenesis (see Fig. 6). There is evidence, however, for significant pressure solution by numerous stylolites observed in several drill cores (for instance B3, B2, A8). This pressure-induced carbonate dissolution is a likely source for ^{13}C-enriched CO_2 admixed to the former organic-derived CO_2 within the Ca2 reservoir rocks of the CO_2-province in the NW-German Basin.

4. Conclusions

The Zechstein 2 (Ca2) carbonate reservoir rocks sampled in 12 drill cores from the CO_2-province of the Lower Saxony Basin in NW-Germany all contain early-formed authigenic minerals which developed in soft sediments as concretions (bending surrounding sediment layers) and/or cementing small cracks, which probably formed during early sediment consolidation (dolomitisation, etc.). The minerals consist mainly of carbonate (mostly calcite and some dolomite) and anhydrite. In contrast to these early formed authigenic minerals numerous cracks and in particular fracture-filling carbonates precipitated during late diagenesis as a consequence of CO_2 degassing induced by local tectonics. These fractures are characterised by sharp contact zones between fracture filling minerals and host rock. The relatively large (up to 2 cm wide) fracture systems were only found in Ca2 rocks containing at present CH_4 as the major gas component. CO_2-rich reservoir rocks show no comparable fracture systems. This suggests variable gas migration situations over short distances (within a range of 2 km) caused by local tectonic events in that particular area.

REE distributions indicate at least three generations of fracture- and crack-filling carbonate. Two groups reflect carbonate formation from different stages of evolving diagenetic fluids whereas the third group (from two CH_4-rich drill sites) indicates a hydrothermal influence sometime during Ca2 history.

The stable carbon isotope compositions of the diagenetic carbonate minerals reflect the carbon sources available during diagenesis. Whereas early diagenetic carbonate minerals (concretions and numerous cracks) are often still related to the Permian (isotopically "heavy") carbon source, organic degradation processes produced isotopically "light" CO_2 near −20‰ which contributed to late diagenetic carbonate cementation. In most cases diagenetic minerals are mixtures between these carbon endmember sources. Diagenetic recrystallisation (crystal enlargement) and subsequent isotope re-equilibration processes are most likely responsible for the low $\delta^{18}O$ values of numerous early-formed diagenetic carbonates. Late diagenetic fracture-filling carbonate, however, precipitated at temperatures up to approximately 100–150 °C. As this fracture-filling carbonate precipitation was most likely caused by CO_2 degassing, the gas content of the Ca2 reservoir rocks was significantly affected in this temperature range. Rb/Sr and U/Pb isotope analyses of carbonate, sphalerite and galena support the idea of late diagenetic/tectonically-induced mineral formation during late stage of (or after) LSB-inversion in Late Cretaceous times.

The relative amount and carbon isotope composition of modern CO_2 within the Ca2 reservoir rocks is extremely variable indicating also at least two CO_2 sources. Similar to the diagenetic carbonates, present day CO_2 concentration data and its carbon isotope values can be explained by mixing of two carbon sources: a ^{12}C-enriched carbon source from organic matter degradation ($\delta^{13}C$ near −20‰) and an isotopically "heavy" carbon source ($\delta^{13}C$ near 0‰). Whereas organic matter degradation processes are well known to have occurred in the Ca2 rocks during diagenesis, the origin of the relatively heavy carbon source is suspected to be related to yet unknown carbonate decomposition processes.

Acknowledgements

We acknowledge the support by the Deutsche Forschungsgemeinschaft (DFG-No. Bo1028/12-1) within the framework of SPP 1135 ("Dynamics of sedimentary systems under varying stress regimes: The example of the Central European Basin"). We thank the companies ExxonMobil, Wintershall and the BGR for supporting us with samples and data. U. Westernströer helped with ICPMS analyses. We are grateful to H. Strauss who reviewed an earlier version of the manuscript. **[LW]**

Appendix A

Table 1A
Mineralogical and geochemical characteristics of authigenic minerals

Drill site	Sample	Depth [m]	Stratigraphy	Sample type	Mineralogy major (minor)	$CaCO_3$ content [%]	$\delta^{13}C$ [‰PDB]	$*\delta^{18}O$ [‰PDB]
B1	-1	2735.5–2752.9	A2	concr.	An (Sid, Fl, Cc)		5.9	−10.3
	-2	2735.5–2752.9	A2	concr.	An (Cc, Fl, Sid)		5.8	−7.4
	-17	2756.9–2764.9	Ca2	concr.	Dol (An, Hal)		6.0	−0.6
	-22	2756.9–2764.9	Ca2	concr.	An, Fl (Hal, Cc)		3.6	−2.6
	-26	2764.9–2777.4	Ca2	concr.	An (Dol, Cc, Hal, Fl)			
	-29	2764.9–2777.4	Ca2	concr.	An, Dol, Cc (Hal, Sid, Fl)			
	-30	2764.9–2777.4	Ca2	concr.	An (Hal, Sid, Cel, Bar, Fl, Dol)			
	-30/II	2764.9–2777.4	Ca2	concr.	An, Fl (Hal, Cc)		5.1	−0.8
	-33	2764.9–2777.4	Ca2	concr.	An (Fl, Cc)		5.5	−0.1
	-34	2764.9–2777.4	Ca2	concr.	An, Cc (Hal, Fl)		−1.8	−10.1
	-35	2764.9–2777.4	Ca2	concr.	An (Dol, Fl, Hal)			
	-36	2764.9–2777.4	Ca2	concr.	An, Fl (Hal, Cc)		5.3	−0.3
	-37	2764.9–2777.4	Ca2	concr.	An, Carb (Fl, Sid)		5.7	−0.5
	-37/II	2764.9–2777.4	Ca2	concr.	An (Fl, Sid)			
	-38	2764.9–2777.4	Ca2	concr.	An, Fl (Sid, Cc)		4.9	−0.9
	-39	2764.9–2777.4	Ca2	concr.	An, Dol (Cc, Fl, Hal)			
	-41a	2764.9–2777.4	Ca2	crack	Dol, An			
	-43	2764.9–2777.4	Ca2	crack	An (Dol, Fl, Hal, Cc)		4.0	−2.2
	-44	2764.9–2777.4	Ca2	concr.	An, Fl (Hal)			
	-44/II	2764.9–2777.4	Ca2	concr.	An (Fl, Sid, Cc)		5.8	0.6
A1	-1	3191–3192.33	Ca2	concr.	An, Cc, Dol (Sid, Sul, Fl)		−3.4	−13.9
	-1/II	3191–3192.33	Ca2	concr.	An (Fl, Sid, Cc)		5.2	−3.3
	-1/III	3191–3192.33	Ca2	crack	Cc, An (Dol)		−2.6	−10.1
	-2	3230.25–3232.13	Ca2		An, Cc (Dol, Sid, Bar, Fl)	10	−2.1	−11.5
	-2/II	3230.25–3232.13	Ca2	crack	An, Cc, Fl (Sid)		−2.3	−9.3
	-2/III	3230.25–3232.13	Ca2	concr.	An, Cc (Fl, Sid)		−1.1	−11.7
A2	-Z9-II	3089.51–3091.47	Ca2	crack	Fl, Cc, An (Dol)		−7.4	−12.0
A3	-1	3384.04–3384.91	Ca2	concr.	Cc (Dol)		−0.3	−10.0
	-1/II	3384.04–3384.91	Ca2	concr.	Cc (Dol, Pyr)		−8.5	−10.4
	-2a	3384.91–3385.85	Ca2	crack	Cc (Dol, Hal)		−0.3	−8.8
	-2b	3384.91–3385.85	Ca2	crack	Cc (Dol, Hal, Pyr)		2.0	−7.9
	-3b	3385.85–3386.79	Ca2	concr.	Cc, Dol (Pyr, Qz)	95	0.1	−8.3
	-3a	3385.85–3386.79	Ca2	concr.	Cc (Pyr, Qz)	95	−2.2	−10.7
	-3/II	3385.85–3386.79	Ca2	concr.	Cc (Fl, Dol)		−0.9	−10.3
	-4	3388.64–3389.58	Ca2	crack	Cc, Dol (Hal, Pyr, An)		0.2	−9.5
	-5	3391.45–3392.23	Ca2	concr.	Cc (Pyr, Dol)		0.5	−9.2
	-6a	3394–3394.93	Ca2	concr.	Cc (Cel, Bar, Fl, Dol)	97	−3.3	−9.7
	6a-1						0.1	−8.9
	6a-2						0.5	−8.8
	6a-3						−0.6	−9.1
	6a-4						−1.8	−9.2
	6a-5						0.3	−8.9
	6a-6						0.6	−8.9
	6a-7						0.1	−9.0
	6a-8						0.0	−8.9
	6a-9						0.5	−8.9

(continued on next page)

Table 1A (*continued*)

Drill site	Sample	Depth [m]	Stratigraphy	Sample type	Mineralogy major (minor)	$CaCO_3$ content [%]	$\delta^{13}C$ [‰PDB]	$*\delta^{18}O$ [‰PDB]
A3	6a-10						0.2	−8.9
	6a-11						−1.5	−9.2
	6a-12						−3.0	−9.4
	6a-13						−3.1	−9.4
	6a-14						−5.2	−10.3
	-6b	3394–3394.93	Ca2	concr.	Cc (Fl, Dol)		0.3	−9.0
	-6b/II	3394–3394.93	Ca2	concr.	Fl (An, Dol, Pyr)			
	-6b/III	3394–3394.93	Ca2	concr.	Cc, Fl (Dol)			
	-7	3395.88–3396.78	Ca2	concr.	Cc (Dol)		−0.1	−9.7
	-7/II	3395.88–3396.78	Ca2	concr.	Cc (Fl)		−2.7	−9.9
	-8/II	3398.66–3399.61	Ca2	concr.	Cc (An, Pyr, Dol)		−4.5	−12.5
	-9/II	3399.61–3400.56	Ca2	concr.	Cc (An, Dol)		−5.0	−12.9
	-9/III	3399.61–3400.56	Ca2	concr.	Cc (Qz)	98	−7.0	−11.5
A4	-1	2880.27–2881.22	Ca2	concr.	Cc (Dol, An, Pyr)	92	2.0	−8.8
	-2a/II-b	2884.05–2884.98	Ca2	crack	Dol, Cc (Sul)	97	1.4	−10.0
	-2a/II-a	2884.05–2884.98	Ca2	crack	Cc (Sul)	97	−4.6	−13.5
	-2b	2884.05–2884.98	Ca2	fract.	Cc (Dol)		−5.9	−13.3
	2b-1						−6.5	−13.4
	2b-2						−4.9	−13.2
	2b-3						−5.8	−13.2
	2b-4						−6.4	−13.4
	2b-5						−4.2	−12.8
	2b-6						−4.9	−13.0
	2b-7						−6.5	−13.4
	-3/II	2888.66–2889.6	Ca2	crack	Cc, Dol	96	−1.2	−11.7
	-3/III	2888.66–2889.6	Ca2	crack	Cc		5.4	−5.2
	-3/IV	2888.66–2889.6	Ca2	crack	Dol (Cc, Hal, Pyr)		−0.1	−10.5
	-4/II	2890.55–2891.45	Ca2		Dol, Cc		−1.3	−11.8
	-5	2895.26–2896.21	Ca2	crack	Dol (Cc, Qz)	94	−1.5	−11.2
	-6	2897.16–2898.1	Ca2	crack	Dol (An, Cc)	98	−0.8	−10.2
	-6/II	2897.16–2898.1	Ca2	crack	Dol (Fl, Cc)		−0.1	−11.3
	-7	2914.62–2915.53	Ca2	concr.	Cc (Fl, Pyr, Dol)		1.3	−9.8
	-7/II-a	2914.62–2915.53	Ca2	concr.	Cc (Pyr, An)		1.1	−7.5
	-7/II-b	2914.62–2915.53	Ca2	concr.	Cc, Dol (Pyr, An)		−1.2	−8.2
	-7/III	2914.62–2915.53	Ca2	concr.	Cc (An, Pyr, Dol)		−1.4	−9.6
	-8	2917.4–2918.3	Ca2	concr.	An (Cc, Sid, Fl)	16	3.4	−6.0
	-8/II	2917.4–2918.3	Ca2	concr.	Cc, An		−0.2	−8.4
	-8/III	2917.4–2918.3	Ca2	concr.	Cc, An (Fl, Sid)		−0.1	−8.2
	-/IV	2917.4–2918.3	Ca2	crack	Cc (An)		2.4	−8.4
	-9a	2925.09–2926.01	Ca2	concr.	Cc (Dol)		0.4	−9.7
	-9b	2925.09–2926.01	Ca2		Cc, Dol (Pyr, Sul)	96	2.3	−9.1
	-9b/II	2925.09–2926.01	Ca2		Cc (Qz, Dol)		−1.0	−9.6
	-10a	2926.01–2926.92	Ca2	crack	Cc (Dol, Hal, Fl, An)	94	1.0	−10.0
	-10a/II	2926.01–2926.92	Ca2		Dol (Cc, Hal, Pyr, Fl)		−0.7	−8.4
	-10a/III	2926.01–2926.92	Ca2		Fl, An (Dol, Cc)		−1.1	−10.7
	-10b	2926.01–2926.92	Ca2		Dol, Cc, An (Hal, Pyr)	40	−0.7	−11.2
	-11/Il-a	2927.83–2928.74	Ca2	concr.	Cc		−2.0	−10.9
	-11/Il-b	2927.83–2928.74	Ca2	concr.	Cc, Dol		−1.1	−8.0
	-12	2929.63–2930.5	Ca2	crack	An, Dol (Cc, Fl, Sid)	26	−0.6	−11.0
	-13	2931.59–2932.43	Ca2	crack	Cc, An	91	−0.4	−8.6
	-13/II	2931.59–2932.43	Ca2	crack	Cc, An (Dol)		0.6	−8.4
	-13/III	2931.59–2932.43	Ca2	concr.	An (Fl, Hal, Cc)		−0.8	−10.3
	-14	2933.33–2934.2	Ca2	concr.	Cc, Dol (Fl, Pyr)		−1.8	−10.7

Table 1A (*continued*)

Drill site	Sample	Depth [m]	Stratigraphy	Sample type	Mineralogy major (minor)	$CaCO_3$ content [%]	$\delta^{13}C$ [‰PDB]	$*\delta^{18}O$ [‰PDB]
A5	-1	3428.7–3437.3	Ca2	crack	Cc (Bar, Hal, Sid)	89	−2.7	−12.6
	-1/II	3428.7–3437.3	Ca2	crack	Cc, Fl (Hal)		−1.9	−11.2
	-2	3428.7–3437.3	Ca2	fract.	Cc	98	1.1	−9.3
	2a-1						1.5	−9.5
	2a-2						−1.0	−9.2
	2a-3						1.7	−9.1
	2a-4						1.1	−9.6
	2a-5						1.4	−9.6
	2a-6						1.6	−8.9
	2a-7						1.9	−8.8
	2a-8						1.4	−9.2
	2a-9						1.6	−9.5
	2a-10						1.5	−9.2
	2a-11						1.7	−8.9
	2a-12						1.8	−8.8
	-2b	3428.7–3437.3	Ca2	fract.	Cc (Dol)		−2.0	−11.3
	2b-1						−3.9	−12.6
	2b-2						−4.0	−12.2
	2b-3						−2.3	−12.1
	2b-4						−3.6	−12.3
	2b-5						−3.6	−12.6
	2b-6						−3.8	−12.7
	-3a	3461.3–3470.5	Ca2	crack	Cc (Dol)		1.6	−9.7
	-3b	3461.3–3470.5	Ca2	crack	Cc (Dol, Pyr)	93	−0.7	−10.4
	-3b/II	3461.3–3470.5	Ca2	crack	Cc (Pyr)		−0.9	−10.4
	-3c	3461.3–3470.5	Ca2	concr.	Cc, Fl (Dol, Pyr)	97	0.2	−9.8
	-4	3461.3–3470.5	Ca2	crack	Cc (Pyr, Dol)		1.0	−9.7
	-5a	3473.5–3481.3	Ca2	crack	Cc, Dol		1.9	−8.6
	-5b	3473.5–3481.3	Ca2	crack	Cc, Dol (Hal)		0.2	−10.3
	-6	3473.5–3481.3	Ca2	fract.	Cc (Dol)		0.4	−9.8
	-6/Il-a	3473.5–3481.3	Ca2	crack	Cc		0.3	−9.2
	-6/Il-b	3473.5–3481.3	Ca2	crack	Cc, Dol		0.9	−7.6
	-6/III	3473.5–3481.3	Ca2	crack	Dol, Cc (Hal)		2.0	−9.4
	-7	3484.3–3493.5	Ca2	crack	Cc (Dol, Hal)		1.0	−11.1
	-7/II	3484.3–3493.5	Ca2	crack	Cc (Dol)		−0.5	−10.9
	-8a	3484.3–3493.5	Ca2	crack	Fl, Dol (An, Cc)	0	5.3	−4.5
	-8/II	3484.3–3493.5	Ca2	crack	An, Fl (Sid)			
	-8b	3484.3–3493.5	Ca2	crack	Fl, Cc (Dol, An)	0	3.0	−7.8
	-8c	3484.3–3493.5	Ca2	crack	An, Fl, Dol (Cc)	1	5.4	−4.2
	-9	3484.3–3493.5	Ca2	crack	Fl (Dol, Cc, An)	0	0.3	−9.6
A6	-1a	3568.6–3577.1	Ca2	crack	Cc, Fl (Dol)	80	−1.5	−10.5
	-1a/II	3568.6–3577.1	Ca2	crack	Cc, Fl (Dol)		−3.1	−11.4
	-1b	3568.6–3577.1	Ca2	crack	Cc (Dol, Fl, Qz)	98	−1.8	−10.6
	-2a	3577.1–3578.4	Ca2	crack	Cc, Fl (Dol, An, Hal, Bar, Qz, Pyr)		−3.1	−11.4
	-2a/II	3577.1–3578.4	Ca2	crack	Cc		−0.8	−10.3
	-2b	3577.1–3578.4	Ca2	crack	Cc		−3.0	−11.2
	-2b/II	3577.1–3578.4	Ca2	crack	Cc (Bar)		−3.7	−11.4
B2	-3	3288.68	Ca2	concr.	Cc, Fl (Hal, Pyr)		−2.2	−12.9
	-4	3290.31	Ca2	concr.	Cc, Dol (Hal, Pyr, Fl)		−1.9	−12.5
	-12	3295.74	Ca2	crack	Cc, Dol (An, Hal)		2.4	−9.7
	-14	3296.92	Ca2	crack	Cc, Dol, Fl (Hal, An)		2.1	−10.1
	-18	3298.82	Ca2	concr.	An (Dol, Cc, Fl, Bar, Hal, Pyr, S)		−1.6	−13.8
	-18/II	3298.82	Ca2	concr.	An (Dol, Cc)		4.5	−4.0

(continued on next page)

Table 1A (*continued*)

Drill site	Sample	Depth [m]	Stratigraphy	Sample type	Mineralogy major (minor)	$CaCO_3$ content [%]	$\delta^{13}C$ [‰PDB]	$*\delta^{18}O$ [‰PDB]
B2	-19	3299.47	Ca2	concr.	An, Cc (Dol, Hal, Sid, Fl)		−1.1	−12.1
	-20	3299.63	Ca2	concr.	An, Cc (Dol, Bar, Sul, Hal, Sid, Pyr, Fl)		−0.9	−11.8
	-21/II	3300.28	Ca2	concr.	An, Fl (Hal, Cc)		0.2	−10.5
	-22	3301.87	Ca2	concr.	An (Fl, Sid, Cc)		2.7	−8.7
	-23	3306.67	Ca2	concr.	An (Fl, Sid)			
	-24	3307.65	Ca2	crack	Dol, An (Cc, Hal, Pyr, Fl)		5.6	−1.0
	-25/II	3307.91	Ca2	concr.	An (Hal, Sid, Fl)			
	-26	3308.13	Ca2	concr.	An (Hal, Sid, Fl)			
	-26/II	3308.13	Ca2	concr.	An, Hal (Fl)			
	-27	3308.93	Ca2	concr.	An, Hal, Sid (Fl)			
	-28	3309.3	Ca2	concr.	Dol, An (Cc, Pyr, Qz, Sul, Fl)		4.2	−4.9
	-29	3311.25	Ca2	concr.	Cc, Fl (Hal, An, Dol)		−0.6	−8.8
	-30	3311.56	Ca2	concr.	An, Cc (Dol, Bar, Hal, Sid, Fl)		−1.4	−12.4
	-31	3312.35	Ca2	concr.	An, Dol, Cc (Fl, Hal)		0.6	−7.9
	-31/II	3312.35	Ca2	concr.	An, Cc (Hal, Sid, Fl)		−2.5	−8.8
	-32	3312.4	Ca2	concr.	An (Cc, Sid, Fl)		−0.9	−11.7
	-33	3313.81	Ca2	concr.	An, Cc (Hal, Fl)		0.3	−11.1
	-0	3313.16–3315.03	Ca2	concr.	An (Bar, Sid, Pyr, Sul, Cc)	3		
	-35	3315.98	Ca2	concr.	Cc, An (Dol, Fl, Hal)		2.6	−8.5
	-36	3316.84	Ca2	concr.	An (Fl, Hal, Cc)		4.2	−4.1
	-36/II	3316.84	Ca2	concr.	An (Hal, Sid, Pyr, Fl, Cc)		1.5	−8.7
	-37	3317.65	Ca2	concr.	Cc, An (Dol)		−5.7	−11.3
	-38/II	3318.3	Ca2	concr.	An, Fl (Hal, Cc)		5.2	−4.2
	-39	3319.77	Ca2	concr.	Cc, An, Hal		−2.0	−8.8
	-39/II	3319.77	Ca2	concr.	An, Cc (Fl, Sid)		2.1	−11.1
	-39/III	3319.77	Ca2	concr.	Cc, An (Dol, Hal)		−4.9	−9.1
	-39/IV	3319.77	Ca2	concr.	Cc, An (Dol, Hal)		−0.6	−9.9
B3	-3	2970.77	Ca2	concr.	Cc, Fl		3.3	−6.7
	-5	2972.72	Ca2	concr.	Cc (Dol)		3.7	−3.1
	-9	2976.12	Ca2	concr.	Fl, Cc (An, Qz)		4.6	−4.4
	-9/II	2976.12	Ca2	concr.	Cc, Fl		1.4	−7.1
	-9/III	2976.12	Ca2	concr.	Fl (Cc)		3.8	−5.2
	-10	2976.79	Ca2	crack	Cc (Fl)		1.7	−5.4
	-11	2978.11	Ca2	concr.	Fl, Cc (Bar, Cel)		0.9	−7.0
	-14	2981.67	Ca2	concr.	Cc, Fl (Dol)		3.3	−7.6
	-15	2982.17	Ca2	concr.	Cc (Dol, Qz)		4.2	−8.0
	-15/II	2982.17	Ca2	concr.	Fl, Cc (Dol)		4.0	−8.0
	-17	2984.27	Ca2	concr.	Fl, Cc (An, Dol)		2.8	−8.2
	-20	2985.96	Ca2	crack	Cc, Fl (Dol)		2.8	−9.5
	-22	2986.99	Ca2	crack	Cc, Fl (Dol, Hal)		3.4	−9.6
	-23	2987.42	Ca2	crack	Cc, Fl (Dol)		−2.0	−8.7
	-25	3002.14	Ca2		Sul			
	-26	3002.96	Ca2	crack	Cc (Fl, Bar, Dol)		3.0	−9.3
	-28	3005.37	Ca2		Sul			
	-30	3007.14	Ca2		Sul			

Table 1A (*continued*)

Drill site	Sample	Depth [m]	Stratigraphy	Sample type	Mineralogy major (minor)	$CaCO_3$ content [%]	$\delta^{13}C$ [‰PDB]	$*\delta^{18}O$ [‰PDB]
B3	-31	3007.63	Ca2		Sul			
	-32	3008.03	Ca2		Sul			
	-34	3009.53	Ca2		Sul			
	-35	3009.89	Ca2	concr.	Cc (Fl, Hal, Dol)		3.7	−7.8
	-36	3012.28	Ca2	crack	Fl, Cc (Dol)		5.0	−9.8
	-38	3014.89	Ca2	crack	Fl, Cc (Dol)		3.8	−9.1
	-40	3016.67	Ca2	crack	Cc, Dol (Hal, Qz)		5.3	−7.5
	-40/II	3016.67	Ca2	crack	Cc (Dol)		5.3	−6.7
	-41a	3017.53	Ca2	crack	Cc (Hal, Dol)		1.2	−7.6
	-41a/II	3017.53	Ca2	concr.	Cc (Dol)		3.3	−9.1
	-41b	3017.53	Ca2	crack	Cc (Dol)		1.5	−7.8
	-41c	3017.53	Ca2		Cc (Hal, An, Dol)		1.4	−8.2
	-42	3018.4	Ca2	crack	Cc (Dol)		6.0	−4.0
	-43	3019.4	Ca2	crack	Cc, Fl (Dol, Hal)		4.3	−8.5
	-44	3019.96	Ca2	concr.	Cc, Fl (Dol, An, Hal,Cel)		3.6	−8.1
	-44/II	3019.96	Ca2	concr.	Fl, Cc, An (Dol, Cel, Pyr)		1.4	−8.2
	-45	3020.77	Ca2		Cc, Fl (Dol, An)		4.4	−6.4
	-47	3022.32	Ca2	crack	Cc, Fl (Dol)		4.1	−8.1
	-48	3022.68	Ca2	concr.	Cc (Dol)		6.2	−2.1
	-48/II	3022.68	Ca2	concr.	Cc (Dol)		4.6	−6.7
	-48/III	3022.68	Ca2	concr.	Cc (Dol)		3.6	−7.3
	-48/IV	3022.68	Ca2	crack	Cc (Dol)		2.6	−6.1
	-49	3023.33	Ca2	crack	Cc (Hal, An, Dol)		6.1	−0.8
	-50	3023.62	Ca2	concr.	Cc (Dol)		1.6	−7.3
	-51	3024.33	Ca2	crack	Cc (Dol)		5.9	−1.0
	-51/II	3024.33	Ca2	crack	Cc (Cel, Bar, Pyr, An)		5.7	−5.4
	-52	3024.55	Ca2	crack	Cc (Cel, Bar, Qz, Hal, Dol)		5.4	−4.7
	-54	3026.48	Ca2	concr.	Cc, Fl, An (Dol, Cel, Bar)		3.1	−6.4
	-55	3027.09	Ca2	concr.	An, Cc (Cel, Bar, Hal, Fl)		1.9	−5.8
	-56	3027.45	Ca2	concr.	An, Cc (Fl)		1.7	−6.3
	-57	3028.00	Ca2	concr.	An (Cc, Fl, Cel, Sid)		2.9	−6.4
	-58	3028.84	Ca2	crack	An, Cc (Dol, Fl, Hal)		5.9	−6.2
	-58/II	3028.84	Ca2	concr.	An, Cc (Fl, Hal)		2.2	−6.9
	-59	3029.04	Ca2	crack	An, Cc (Fl, Hal)		5.7	−5.9
	-59/II	3029.04	Ca2	concr.	An (Cc, Fl, Hal)		2.5	−7.2
	-59/III	3029.04	Ca2	concr.	An, Cc (Dol, Hal, Fl)		1.0	−7.0
	-60	3029.8	Ca2	concr.	An, Cc (Cel, Hal, Fl)		3.0	−6.9
	-61a	3030.13	Ca2	concr.	Cc (Cel, Bar, Qz, Fl, An)		1.5	−6.1
	-61b	3030.13	Ca2	concr.	Dol, Cc (Cel, Bar, Qz, Fl, An)		5.5	−2.2
	-61/II	3030.13	Ca2	crack	Cc, An (Dol, Cel, Bar, Fl)		2.3	−7.1
	-62	3030.73	Ca2	crack	Cc (Hal, Qz, An, Dol)		6.1	−1.6
	-62/II	3030.73	Ca2	concr.	An, Cc (Fl, Hal)		3.2	−5.5
	-63	3030.82	Ca2	concr.	An, Cc (Cel, Sid, Fl)		5.1	−5.3

(continued on next page)

Table 1A (*continued*)

Drill site	Sample	Depth [m]	Stratigraphy	Sample type	Mineralogy major (minor)	$CaCO_3$ content [%]	$\delta^{13}C$ [‰PDB]	$*\delta^{18}O$ [‰PDB]
B3	-64	3030.9	Ca2	concr.	Cc (Cel, Bar, Fl, An)		0.3	−8.3
	-64/II	3030.9	Ca2	concr.	Cc (Fl, Qz, Dol)		4.9	−3.4
	-64/III	3030.9	Ca2	concr.	An, Cc (Fl, Hal)		4.8	−7.1
	-64/IV	3030.9	Ca2	crack	Cc (An, Dol)		6.2	−0.3
	-65	3031.31	Ca2	crack	An, Cc, Dol (Cel, Bar, Sid)		0.4	−6.7
	-66a	3032.38	Ca2	concr.	Cc, An (Cel, Bar, Dol)		1.6	−6.5
	-66/II	3032.94	Ca2	concr.	Cc (Cel, Bar, An, Dol)		0.9	−6.4
	-66/2	3032.94	Ca2	crack	Cc, Fl (Dol)		5.3	−6.4
	-68	3033.97	Ca2		Sul			
	-70	3035.79	Ca2	crack	Cc (Fl, Qz)		1.3	−6.8
	-70/II	3035.79	Ca2	crack	Cc, Fl (Dol)		4.6	−6.6
	-71	3036.06	Ca2	crack	Cc (Hal, Fl, Dol)		5.4	−6.7
	-71/II	3036.06	Ca2	crack	Cc (Fl, Dol)		3.8	−7.0
	-72	3036.26	Ca2	crack	Cc, Fl (Dol)		3.9	−7.0
A7	-1	2968.44–2969.8	Ca2	crack	Cc (Dol)		−3.4	−12.2
	-2a	2972.47–2973.39	Ca2	concr.	Cc (Dol)		−3.3	−11.9
	-2b	2972.47–2973.39	Ca2	concr.	Cc (An, Dol)		5.5	−2.7
	-2b/II	2972.47–2973.39	Ca2	concr.	Cc (An, Qz, Dol)		4.3	−3.4
	-3	2978.26–2979.26	Ca2	concr.	Cc (Dol)		0.3	−6.7
	-3/II	2978.26–2979.26	Ca2	concr.	Cc (An)		−0.5	−7.8
	-4a	2982.13–2983.13	Ca2	concr.	Cc (Hal, Dol)	96	0.5	−8.0
	-4a/II	2982.13–2983.13	Ca2	concr.	Cc, Fl (An)		1.0	−8.8
	-4b	2982.13–2983.13	Ca2	concr.	Cc (Dol)		0.0	−8.2
	-5	2997.23–2998.21	Ca2	concr.	Cc (Fl)		6.4	−1.7
	-5/II	2997.23–2998.21	Ca2	concr.	Cc, Fl (Dol)		3.0	−5.6
	-6	3000.06–3001.04	Ca2	concr.	An, Cc (Hal, Pyr)		5.4	−7.6
	-7a	3001.04–3001.9	Ca2	crack	Cc (Hal, Dol)		5.4	−9.1
	-7a/II	3001.04–3001.9	Ca2	crack	Cc, An (Dol)		4.5	−7.0
	-7b	3001.04–3001.9	Ca2	crack	Cc, An (Hal, Sid, Pyr)	97	2.6	−7.0
	-8	3002.3–3002.81	Ca2	crack	Cc (An, Hal, Dol)	96	3.3	−7.5
	-8/II	3002.3–3002.81	Ca2	crack	An, Cc (Hal, Pyr, Sul, Fl)		2.3	−8.0
	-8/III	3002.3–3002.81	Ca2	crack	Cc (An, Dol)		5.3	−4.9
	-8/IV	3002.3–3002.81	Ca2	crack	Cc (Dol)		5.5	−5.8
	-9	3002.81–3003.76	Ca2	concr.	Cc, Dol (Hal)		7.2	−1.3
	-10/2	3008.41–3009.28	Ca2	crack	Cc, Fl (Hal, Pyr, An)	81	4.8	−6.3
	-11	3013.92–3014.84	Ca2	crack	Cc, Fl (Dol)		5.5	−7.1
	-12	3018.51–3019.39	Ca2	concr.	Cc		2.0	−6.3
	-12/II	3018.51–3019.39	Ca2	concr.	Cc, An (Bar, Hal)		3.0	−4.9
	-13	3023.19–3024.06	Ca2	crack	Cc (Dol, An)	93	5.8	−3.4
	-14a	3025–3025.97	Ca2	crack	Cc (Dol)		5.6	−3.0
	14a-1						6.1	−2.4
	14a-2						6.0	−6.2
	14a-3						6.0	−7.1
	14a-4						5.5	−4.0
	-14a/II	3025–3025.97	Ca2	concr.	An, Cc (Fl, Hal)		3.1	−6.7
	-14a/III	3025–3025.97	Ca2	crack	Cc		5.8	−1.5
	-14b	3025–3025.97	Ca2	concr.	Cc (Dol)		5.4	−6.0
	-14b/II	3025–3025.97	Ca2	concr.	An, Cc (Cel, Hal, Fl)		2.6	−7.4
	-14b/III	3025–3025.97	Ca2	crack	Cc		6.0	−3.1

Table 1A (*continued*)

Drill site	Sample	Depth [m]	Stratigraphy	Sample type	Mineralogy major (minor)	$CaCO_3$ content [%]	$\delta^{13}C$ [‰PDB]	$*\delta^{18}O$ [‰PDB]
A7	-15	3025.97–3026.88	Ca2	crack	Cc (Dol)		6.0	−0.4
	-16	3033.6–3034.4	Ca2	crack	Cc (An, Dol)		5.8	−3.1
A8	-1a	2990–2990.94	Ca2	crack	Cc		−0.6	−6.6
	-1a/II	2990–2990.94	Ca2	crack	Cc (Fl, Pyr)		−2.1	−7.4
	-1b	2990–2990.94	Ca2	fract.	Cc		−2.2	−8.4
	-1c	2990–2990.94	Ca2	crack	Cc		−0.4	−6.1
	-1c/II	2990–2990.94	Ca2	crack	Cc		2.2	−6.5
	-2	2991.92–2992.83	Ca2	crack	Cc, Fl			
	-2/II	2991.92–2992.83	Ca2	concr.	Cc, Fl		1.6	−6.6
	-3	2992.83–2993.76	Ca2	fract.	Cc		−2.0	−8.4
	-4a	2994.68–2995.67	Ca2	crack	Cc	~100	1.1	−7.2
	-4b	2994.68–2995.67	Ca2	crack	Cc (Dol)		−0.5	−6.6
	-5a	2996.81–2997.48	Ca2	crack	Cc		2.8	−7.5
	-5b	2996.81–2997.48	Ca2	crack	Cc		−0.1	−6.6
	-5b/II	2996.81–2997.48	Ca2	crack	Cc		−2.4	−7.7
	-5c	2996.81–2997.48	Ca2	crack	Cc		3.0	−6.7
	-6	3003.65–3004.45	Ca2	crack	Cc		−0.8	−8.5
	6-1						−0.2	−7.6
	6-2						−0.7	−8.4
	6-3						−2.8	−8.7
	6-4						−1.3	−8.7
	6-5						−0.3	−9.0
	6-6						0.0	−9.0
	6-7						3.6	−8.8
	6-8						2.9	−8.4
	6-9						2.3	−7.8
	-7a	3004.45–3005.38	Ca2	crack	Cc		−1.8	−8.4
	7a/II	3004.45–3005.38	Ca2	crack	Cc, Fl		−0.6	−8.5
	-7b	3004.45–3005.38	Ca2	crack	Cc		−0.4	−8.3
	-7b/II	3004.45–3005.38	Ca2	crack	Cc		3.4	−7.7
	-7b/III	3004.45–3005.38	Ca2	concr.	Cc (Fl)		0.7	−6.0
	-7c	3004.45–3005.38	Ca2	crack	Cc		−2.3	−8.9
	7c-1						2.4	−7.5
	7c-2						0.9	−8.3
	7c-3						1.4	−8.1
	7c-4						0.3	−7.6
	-8a	3005.38–3006.22	Ca2	crack	Cc, Fl		4.1	−7.7
	-8a/II	3005.38–3006.22	Ca2	crack	Fl, Cc		1.0	−7.4
	-8a/III	3005.38–3006.22	Ca2	crack	Cc (Fl)		2.4	−7.9
	-8b	3005.38–3006.22	Ca2	fract.	Cc (Qz)		−2.3	−9.4
	-8c	3005.38–3006.22	Ca2	fract.	Cc		−2.7	−9.8
	-9	3006.22–3007.1	Ca2	fract.	Cc		−3.6	−10.8
	-10	3007.1–3008	Ca2	fract.	Cc		−4.8	−11.2
	-11	3009–3009.94	Ca2	fract.	Cc		−1.9	−10.7
	-12	3009.94–3010.39	Ca2	fract.	Cc (Fl)	95	−4.0	−10.4
	-13	3010.39–3011.83	Ca2	fract.	Cc (Dol, Fl)	83	−3.9	−11.1
	-14	3011.83–3012.72	Ca2	fract.	Cc		−3.5	−11.0
	-15	3013.57–3014.42	Ca2	fract.	Cc (Fl)	96	−1.7	−11.1
	-16	3014.42–3015.31	Ca2	fract.	Cc		−3.1	−11.3
	-17	3015.31–3016.26	Ca2	fract.	Cc		−1.5	−10.8
	-18	3017.97–3018.94	Ca2	crack	Cc		3.1	−8.6
	-19a	3018.94–3019.9	Ca2	crack	Cc		1.6	−8.7
	-19a/II	3018.94–3019.9	Ca2	fract.	Cc (Dol)		−1.3	−11.1
	-19b	3018.94–3019.9	Ca2	concr.	Cc		3.5	−8.9
	-19b/II	3018.94–3019.9	Ca2		Cc, Fl		3.2	−8.7
	-19b/III	3018.94–3019.9	Ca2	crack	Cc (Dol)		−1.5	−11.1

(continued on next page)

Table 1A (*continued*)

Drill site	Sample	Depth [m]	Stratigraphy	Sample type	Mineralogy major (minor)	$CaCO_3$ content [%]	$\delta^{13}C$ [‰PDB]	$*\delta^{18}O$ [‰PDB]
A8	-20	3019.9–3020.88	Ca2	fract.	Cc		−2.7	−11.1
	-21a	3022.8–3023.72	Ca2	fract.	Cc		−1.8	−11.2
	-21a/II	3022.8–3023.72	Ca2	fract.	Cc		0.1	−10.5
	-21b	3022.8–3023.72	Ca2	fract.	Cc		−1.9	−11.7
	-21c	3022.8–3023.72	Ca2	fract.	Cc		−1.1	−9.2
	-22	3023.72–3024.65	Ca2	fract.	Cc		−2.6	−12.1
	-23a	3028.99–3029.95	Ca2	fract.	Cc		−1.2	−11.5
	-23a/II	3028.99–3029.95	Ca2	fract.	Cc (Fl)		−2.7	−11.8
	-23b	3028.99–3029.95	Ca2	fract.	Cc, Fl	73	−2.8	−11.4
	-24a	3032.95–3033.95	Ca2	crack	Cc, Dol (An)		−3.3	−11.3
	-24a/II	3032.95–3033.95	Ca2	crack	Cc (Dol)		−1.9	−12.2
	-24a/III	3032.95–3033.95	Ca2	concr.	Cc (Dol)		−0.8	−7.1
	-24b	3032.95–3033.95	Ca2	fract.	Cc		−1.6	−12.0
	24b-1						−2.4	−11.6
	24b-2						−2.2	−11.9
	24b-3						−2.5	−11.8
	24b-4						−1.3	−11.4
	-24b/III	3032.95–3033.95	Ca2	fract.	Cc (Dol)		−0.7	−11.2
	-25	3037.24–3038.06	Ca2	fract.	Fl, Cc	30	−3.6	−11.0
	-26	3068.95–3069.9	Ca2	crack	Cc (Fl)		−4.6	−11.2
	-26/II	3068.95–3069.9	Ca2	concr.	Cc (Dol)		0.8	−8.8
A9	-1	3233.65–3234.6	Ca2	crack	Fl (Cc, Pyr)	0		
	-1/II	3233.65–3234.6	Ca2	crack	Fl (Dol)			
	-2a	3241.8–3242.7	Ca2	crack	Cc		−1.7	−8.8
	-2b	3241.8–3242.7	Ca2	crack	Cc	97	−1.8	−9.1
	-2b/II	3241.8–3242.7	Ca2	crack	Cc		−4.4	−8.3
	-3	3246.47–3247.42	Ca2	crack	Cc (An)		1.0	−7.3
	-3/II	3246.47–3247.42	Ca2	crack	Cc (Fl)		1.7	−7.8
	-4	3248.34–3249.23	Ca2	crack	Cc		−3.7	−7.5
	-5a	3252.02–3253.01	Ca2	fract.	Cc		−6.0	−8.7
	5a-1						−7.7	−9.9
	5a-2						−6.3	−10.0
	5a-3						−6.8	−9.5
	5a-4						2.3	−6.0
	5a-5						−6.3	−6.9
	5a-6						−7.5	−7.6
	-5b	3252.02–3253.01	Ca2		Cc		−1.7	−10.7
	-5b/II	3252.02–3253.01	Ca2	crack	Cc (Dol)		5.1	−8.8
	-5b/III	3252.02–3253.01	Ca2		Cc (Fl)		−2.0	−9.2
	-6	3253.96–3254.92	Ca2	crack	Cc (Fl)	97	0.4	−8.9
	-7	3254.92–3255.87	Ca2	crack	Cc (Fl)	97	−2.2	−9.0
	-7/II	3254.92–3255.87	Ca2	crack	Cc (Dol)		−0.9	−8.7
	-8	3256.78–3257.75	Ca2	crack	Cc (An)		−0.1	−8.1
	-9a	3257.75–3258.6	Ca2	crack	Cc		2.7	−6.4
	-9a/II	3257.75–3258.6	Ca2	crack	Cc		0.8	−9.0
	-9b	3257.75–3258.6	Ca2	crack	Cc (Dol)		−1.8	−8.5
	-10	3260.25–3261.22	Ca2	crack	Cc (Dol)		2.3	−7.9
	-10/II	3260.25–3261.22	Ca2	crack	Cc (Dol)		1.4	−7.8
	-11	3271.1–3272.02	Ca2	crack	Cc		6.5	−1.1
	-11/II	3271.1–3272.02	Ca2	concr.	Fl, Cc (Dol)		2.6	−9.6

Sample type: concr. = concretion, fract. = fracture.

Mineralogical compounds determined by XRD: Anhydrite (An), Baryte (Bar), Calcite (Cc), Celestine (Cel), Dolomite (Dol), Fluorite (Fl), Halite (Hal), Pyrite (Pyr), Quartz (Qz), Siderite (Sid), Sulfur (Sul).

*Oxygen isotope values of dolomites are corrected after Sharma and Clayton (1965).

References

Alibo, D.S., Nozaki, Y., 1999. Rare earth elements in seawater: particle association, shale−normalization, and Ce oxidation. Geochim. Cosmochim. Acta 63, 363–372.

Allen, P.A., Allen, J.R., 1990. Basin Analysis–Principles and Applications. Blackwell, London. 451 pp.

Bathurst, R.G.C., 1976. Carbonate Sediments and their Diagenesis. Developments in Sedimentology, vol. 12. Elsevier, New York. 658 pp.

Bau, M., Dulski, P., Möller, P., 1995. Yttrium and Holmium in South Pacific Seawater: vertical distribution and possible fractionation mechanisms. Chem. Erde 55, 1–15.

Below, A., 1992. Fazies−und Geochemische Diagenesestudie im Zechstein 2−Karbonat (Ca2) Nordwestdeutschlands. Berichte−Reports Geol.−Paläont. Inst. vol. 60. Christian−Albrechts−Universität, Kiel. 147 pp.

Betz, D., Führer, F., Greiner, G., Plein, E., 1987. Evolution of the Lower Saxony Basin. Tectonophysics 137, 127–170.

Boigk, H., 1981. Erdöl und Erdölgas in der Bundesrepublik Deutschland. Enke Verlag, Stuttgart. 313 pp.

Bottinga, Y., 1969. Calculated fractionation factors for carbon and hydrogen isotope exchange in the system calcite−carbondioxide−graphite−methane−hydrogen−water vapor. Geochim. Cosmochim. Acta 33, 49–64.

Botz, R. 1979. Mineralogie, Geochemie und Isotopengeochemie des Stinkschiefers im Germanischen Becken (Nordwest−Deutschland) PhD thesis, Ruprecht−Karl−Universität, Heidelberg. 225 pp.

Botz, R., Müller, G., 1981. Mineralogie, Petrographie, anorganische Geochemie und Isotopen−Geochemie der Karbonatgesteine des Zechstein. Geol. Jahrb., D 2 (47), 3–112.

Botz, R., Müller, G., 1987. Geochemische Untersuchungen an Karbonaten und organischer Substanz in Karbonatsgesteinen des NW−deutschen Zechstein−Beckens. Chem. Erde 46, 131–143.

Brink, H.J., 2002. Die Anomalie von Bramsche-wieder eine offene Frage? Erdöl Erdgas Kohle 1, 18–22.

Brink, H.J., Dürschner, H., Trappe, H., 1992. Some aspects of the late and post−Variscan development of the Northwestern German Basin. Tectonophysics 207, 65–95.

Brown, A.A., 1999. Distinguishing mantle CO_2 from decarbonation CO_2 in high CO_2 gases. AAPG Hedberg Research Conference "Natural Gas Formation and Occurrence", Durango Colorado.

Büchner, M., 1986. Geothermisch bedingte Veränderungen in Rhät−und Jura−Gesteinen des Unteren Weserberglandes als Folge des Vlothoer Glutfluβmassivs. Ber. Naturwiss. Ver. Bielef. Umgebung 28, 109–138.

Buntebarth, G., 1985. Das Temperaturgefälle im Dach des Bramscher Massivs aufgrund von Inkohlungsuntersuchungen im Karbon von Ibbenbüren. Fortschr. Geol. Rheinl. Westfal. 33, 255–264.

Cathles, L.M., Schoell, M., 1999. CO_2 generation, migration, and titration in sedimentary basins. AAPG Hedberg Research Conference "Natural Gas Formation and Occurrence", Durango Colorado.

Chow, N., Morad, S., Al−Asam, I.S., 1996. Origin of authigenic carbonates in Eocene to Quaternary sediments from the Artic Ocean and Norwegian−Greenland Sea. Proc. Ocean Drilling Program Sci. Res., vol. 151, pp. 415–434. College Station, TX.

Clark, D.N., 1980. The Diagenesis of Zechstein carbonate sediments. Contrib. Sedimentol. 9, 167–203.

Claypool, G.E., Kaplan, I.R., 1974. The origin and distribution of methane in marine sediments. In: Kaplan, I.R. (Ed.), Natural Gases in Marine Sediments. Plenum Press, pp. 99–139.

Clayton, J.L., Spencer, C.W., Koncz, I., Szalay, A., 1990. Origin and migration of hydrocarbon gases and carbon dioxide, Békés Basin, southeastern Hungary. Org. Geochem. 15, 233–247.

DeBaar, H.J.W., Brewer, P.G., Bacon, M.P., Bruland, K.W., 1985. Rare earth elements in the Atlantic and Pacific Oceans. Geochim. Cosmochim. Acta 49, 1551–1558.

Deutloff, O., Teichmüller, M., Teichmüller, R., Wolf, M., 1980. Inkohlungsuntersuchungen im Mesozoikum des Massivs von Vlotho (Niedersächsisches Tektogen). Neues Jahrb. Geol. Paläontol., Monatsh. 6, 321–341.

Douville, E., Bienvenu, P., Charlou, J.L., Donval, J.P., Fouquet, Y., Appriou, P., Gamo, T., 1999. Yttrium and rare earth elements in fluids from various deep−sea hydrothermal systems. Geochim. Cosmochim. Acta 63, 627–643.

Drozdzewski, G., Juch, D., Littke, R., Vieth, A., Wrede, V., 2003. A new map of the Pre−Permian of NW−Germany: depth, structure, coalification. Abstract 250, Int. Congress on Carboniferous and Permian Stratigraphy, Utrecht, The Netherlands.

Düppenbecker, S.J., Welte, D.H., 1989. Effects of heating rates on generation and expulsion of hydrocarbons, Lower Saxony Basin, Federal Republic of Germany. 28th Int. Geol. Conf., Washington, 1425 pp.

Elderfield, H., Graeves, M.J., 1982. The rare earth elements in seawater. Nature 296, 214–219.

Emrich, K., Ehhalt, D.J., Vogel, J.C., 1970. Carbon isotope fractionation during the precipitation of calcium carbonate. Earth Planet. Sci. Lett. 8, 363–371.

Fritz, P., Fontes, J.C., 1986. Handbook of Environmental Isotope Geochemistry. Elsevier, Amsterdam, pp. 1–3. 557 pp.

Fritz, P., Binda, P.L., Folinsbee, F.E., Krouse, H.R., 1971. Isotopic composition of diagenetic siderites from Cretaceous sediments in Western Canada. J. Sediment. Petrol. 41, 282–288.

Füchtbauer, H., Peryt, T., 1980. The Zechstein Basin with emphasis on carbonate sequences. Contrib. Sedimentol. 9, 1–2.

Gale, J.F.W., Laubach, S.E., Marrett, R.A., Olson, J.E., Holder, J., Reed, R.M., 2004. Predicting and characterizing fractures in dolostone reservoirs: using the link between diagenesis and fracturing. In: Braithwaite, C.J.R., Rizzi, G., Darke, G. (Eds.), The Geometry and Petrogenesis of Dolomite Hydrocarbon Reservoirs, Special Publications, vol. 235. Geological Society, London, pp. 177–192.

Garbe-Schönberg, C.-D., 1993. Simultaneous determination of 37 trace elements in 28 international rock standards by ICP−MS. Geostand. Newsl. 17, 81–93.

Garrels, R.M., Perry, E.A., 1974. Cycling of carbon, sulfur and oxygen through geologic time. In: Goldberg, E.D. (Ed.), The Sea: Ideas and Observations on Progress in the Study of the Seas. Wiley, New York, pp. 303–336.

Gerling, P., Geluk, M.C., Kockel, F., Lokhorst, A., Lott, G.K., Nicholson, R.A., 1999. 'NW European Gas Atlas'− new implications for the Carboniferous gas plays in the western part of the Southern Permian Basin. In: Fleet, A.J., Boldy, S.A.R. (Eds.), Petroleum Geology of Northwest Europe: Proceedings of the 5th Conference. Geological Society, London, pp. 799–808.

Glodny, J., Bingen, B., Austrheim, H., Molina, J.F., Rusin, A., 2002. Precise eclogitisation ages deduced from Rb/Sr mineral systematics: The Maksyutov complex, Southern Urals, Russia. Geochim. Cosmochim. Acta 66 (7), 1221–1235.

Haley, B., Klinkhammer, G.P., McManus, J., 2004. Rare earth elements in pore waters of marine sediments. Geochim. Cosmochim. Acta 68, 1265–1279.

Hardie, L.A., 1987. Dolomitization: a critical view of some current views. J. Sediment. Petrol. 57, 166–183.

Hodgson, W.A., 1966. Carbon and oxygen isotope ratios in diagenetic carbonates from marine sediments. Geochim. Cosmocim. Acta 13, 322–334.

Irwin, H., Curtis, C., Coleman, M., 1977. Isotope evidence for source of diagenetic carbonates formed during burial of organic–rich sediments. Nature 269, 209–213.

Johannesson, K.H., Zhou, X., 1999. Origin of middle rare earth element enrichments in acid waters of a Canadian High Arctic lake. Geochim. Cosmochim. Acta 63, 153–165.

Keeling, J.D., 1958. The concentration and isotopic abundance of carbon dioxide in rural areas. Geochim. Cosmochim. Acta 13, 322–334.

Kelts, K.R., McKenzie, J.R., 1982. Diagenetic dolomite formation in Quaternary anoxic diatomaceous muds of Deep Sea Drilling Project Leg 64 Gulf of California. In: Curray, J.R., Moore, D.G. (Eds.), Init. Repts DSDP, pp. 553–569.

Kockel, F., Wehner, H., Gerling, P., 1994. Petroleum systems of the Lower Saxony Basin. AAPG Mem. 60, 573–586.

Kramm, U., Wedepohl, K.H., 1991. The isotopic composition of strontium and sulfur in seawater of Late Permian (Zechstein) age. Chem. Geol. 90, 253–262.

Krouse, H.R., Viau, C.A., Eliuk, L.S., Ueda, A., Halas, S., 1988. Chemical and isotopic evidence of thermochemical sulphate reduction by light hydrocarbon gases in deep carbonate reservoirs. Nature 333, 415–419.

Land, L.S., 1980. The isotopic and trace element geochemistry of dolomite: the state of the art. Spec. Publ. - Soc. Econ. Paleontol. Mineral. 28, 87–110.

Liedmann, W., 1992. Diagenese des Hauptdolomits (Z2, Ca2) im Weser–Ems–Gebiet. BEB Report. BEB Erdgas und Erdöl GmbH, Hannover. 12 pp.

Littke, R., Krooβ, B., Idiz, E., Frielingsdorf, J., 1995. Molecular nitrogen in natural gas accumulations: generation from sedimentary organic matter at high temperatures. AAPG Bull. 79, 410–430.

Lokhorst, A. (Ed.), 1998. NW European Gas Atlas– CD–Rom version.

Love, K.M., Strohmenger, C., 1994. Joint BEB–EPR Diagenesis Study of the Zechstein 2 Carbonate (NW–Germany). An Integrated Multivariate Statistical Approach. TA. No. 9 400 102. BEB, Hannover. 39 pp.

Machel, H.G., Krouse, H.R., Sassen, R., 1995. Products and distinguishing criteria of bacterial and thermochemical sulfate reduction. Geochemistry 10, 373–389.

Magaritz, M., Schulze, K.H., 1980. Carbon isotope anomaly of the Permian period. Contrib. Sedimentol. 9, 269–277.

Magaritz, M., Turner, P., Käding, K., 1981. Carbon isotopic change at the base of the Upper Permian Zechstein sequence. Geol. J. 16, 243–254.

Magaritz, M., Schulze, K.H., Turner, P., Käding, K., 1982. Carbon cycle changes of the Zechstein Sea: isotopic transition zone in the Marl Slate. Nature 297, 389–390.

Marshallsea, S.J., 1995. Thermal history interpretation of samples from nine wells, Saxony Basin, Germany. Geotrack Rep. 567, unpubl.

McKenzie, A.J., 1981. Holocene dolomitization of calcium carbonate sediments from the coastal sabkhas of Abu Dhabi, U.A.E.: a stable isotope study. J. Geol. 89, 185–198.

Morse, J.W., Mackenzie, F.T., 1990. Geochemistry of sedimentary carbonates. Developments in Sedimentology, vol. 48. Elsevier, New York. 707 pp.

Nöth, S., Steinhoff, I., 1995. Diageneseentwicklung des Ca2 (Strassfurt–Karbonat)– unter dem Aspekt der Thermochemischen Sulfatreduktion (TSR). Vorläufiger Bericht. TA. No. 9 500 088. BEB, Hannover.

Northrop, D.A., Clayton, R.N., 1966. Oxygen isotope fractionation in systems containing dolomite. J. Geol. 74, 174–196.

Nozaki, Y., Zhang, J., Amakawa, H., 1997. The fractionation between Y and Ho in the marine environment. Earth Planet. Sci. Lett. 148, 329–340.

O'Neil, J.R., Clayton, R.N., Mayeda, T.K., 1969. Oxygen isotope fractionation between divalent metal carbonates. J. Chem. Phys. 51, 5547–5558.

Pagnier, H.J.M., Van den Belt, F.J.G., Mijnlieff, H.F., Van Bergen, F., Verbeek, J.W., 2003. Carboniferous maps and models–recent developments. Abstract, XVth Int. Congr. on Carboniferous and Permian Stratigraphy. Utrecht, The Netherlands.

Patterson, R.J., Kinsman, D.J.J., 1982. Formation of diagenetic dolomite in coastal sabkha along Arabian (Persian) Gulf. AAPG Bull. 66 (1), 28–43.

Paull, C.K., Chanton, J.P., Neumann, A.C., Martens, J.A., Showers, W., 1992. Indicators of methane–derived carbonates and chemosynthetic organic carbon deposits: examples from Florida escarpment. Palaios 7, 361–375.

Peryt, T.M., Magaritz, M., 1990. Genesis of evaporite– associated platform dolomites: case study of the main dolomite (Zechstein, Upper Permian), Leba elevation, northern Poland. Sedimentology 37, 745–761.

Petmecky, S., Meier, L., Reiser, H., Littke, R., 1999. High thermal maturity in the Lower Saxony Basin: intrusion or deep burial? Tectonophysics 304, 317–344.

Pisciotto, K.A., Mahoney, J.J., 1981. Isotope survey of diagenetic carbonates, deep sea drilling project leg 63. In: Yeats, R.S., Haq, B.U. (Eds.), Initial Reports of the Deep Sea Drilling Project 63. College Station, TX, pp. 595–609.

Poelchau, H., Baker, D.R., Hantschel, T., Horsfield, B., Wygrala, B., 1997. Basin simulation and the design of the conceptual model. In: Welte, D.H., Horsfield, B., Baker, D.R. (Eds.), Petroleum and Basin Evolution. Springer, Berlin, pp. 71–166.

Presley, B.J., Kaplan, I.R., 1968. Changes in dissolved sulfate, calcium and carbonate from interstitial water of near shore sediments. Geochim. Cosmochim. Acta 32, 1037–1049.

Roberts, H.H., Whelan, T., 1975. Methane–derived carbonate cements in barrier and beach sands of a subtropical delta complex. Geochim. Cosmochim. Acta 39, 1085–1089.

Rockenbauch, K., Brauckmann, F., Schäfer, H.-G., Utermöhlen, S., 1998. Das Zechstein 2–Karbonat (Ca2) "Stacked–Reservoir" Play in NW–Deutschland. Erdöl Erdgas Kohle 12, 589–594.

Romanek, C.S., Grossman, E.L., Morse, J.W., 1992. Carbon isotopic fractionation in synthetic aragonite and calcite: effects of temperature and precipitation rate. Geochim. Cosmochim. Acta 56, 419–430.

Romer, R.L., 2001. Isotopically heterogeneous initial Pb and continuous ^{222}Rn loss in fossils: the U–Pb systematics of Brachiosaurus brancai. Geochim. Cosmochim. Acta 65 (22), 4201–4213.

Rullkötter, J., Leythaeuser, D., Horsfield, B., Littke, R., Mann, U., Müller, P.J., Radke, M., Schaefer, R.G., Schenk, H.J., Schwochau, K., Witte, E.G., Welte, D.H., 1988. Organic matter maturation under the influence of a deep intrusive heat source: a natural experiment for quantification of hydrocarbon generation and expulsion from a petroleum source rock (Toarcian shale, northern Germany). Org. Geochem. 13, 847–856.

Sackett, W.M., Brooks, J.M., Bernard, B.B., Schwab, C.R., Chung, H., Parker, R.A., 1979. A carbon inventory for Orca Basin brines and sediments. Earth Planet. Sci. Lett. 44, 73–81.

Schidlowski, M., Eichmann, R., Junge, C.E., 1975. Carbon isotope geochemistry of the Precambrian Lomagundi carbonate province, Rhodesia. Geochim. Cosmochim. Acta 40, 449–455.

Schmitz, U., Wenzlow, B., 1990. Maturity anomalies of the western Lower Saxony Basin in their regional context. Zbl. Geol. Paläont. Teil I 8, 1091–1103.

Senglaub, Y., Littke, R., Brix, M.R., in press. Numerical modelling of burial and temperature history as an approach for an alternative interpretation of the Bramsche anomaly, Lower Saxony Basin. Int. J. Earth Sci. doi:10.1007/s00531-005-0033-y.

Sharma, T., Clayton, R.N., 1965. Measurement of $^{18}O/^{16}O$ ratios of total oxygen of carbonates. Geochim. Cosmochim. Acta 29, 1347–1354.

Shield, G.A., Webb, G.E., 2004. Has the REE composition of seawater changed over geological time? Chem. Geol. 204, 103–107.

Smith, J.T., Ehrenberg, S.N., 1989. Correlation of carbon dioxide abundances with temperature in clastic hydrocarbon reservoirs: relationship to inorganic chemical equilibrium. Mar. Pet. Geol. 6, 129–135.

Stahl, W., 1971. Isotopen−Analysen an Carbonaten und Kohlendioxid−Proben aus dem Einflu(gebiet und der weiteren Umgebung des Bramscher Intrusivs und an hydrothermalen Carbonaten aus dem Siegerland. Fortschr. Geol. Rheinl. Westfal. 18, 429–438.

Steinhoff, I., 1988. Evaluation of H_2S Formation in the Basal Zechstein (Upper Permian of Germany). Dissertation, Univ. Texas at El Paso, El Paso, TX. 177 pp.

Steinhoff, I., Strohmenger, C., 1996. Zechstein−2 carbonate platform subfacies and grain−type distribution (Upper Permian, Northwest Germany). Facies 35, 105–132.

Strohmenger, C., Jäger, G., Mitchell, J.C., Love, K.M., Antonini, M., Gast, R., vandePol, E., Rockenbauch, K., Steffan, M., 1993. An integrated approach to Zechstein Ca2 carbonate reservoir facies prediction in the South Oldenburg area, Upper Permian, Northwest Germany (Abstract). AAPG Bull. 77, 1668.

Strohmenger, C., Antonini, M., Jäger, G., Rockenbauch, K., Strauβ, C., 1996. Zechstein 2 carbonate reservoir facies distribution in relation to Zechstein sequence stratigraphy (Upper Permian, Northwest Germany): an integrated approach. Bull. Cent. Rech. Explor. Prod. Elf-Aquitaine 20 (1), 1–35.

Strohmenger, C., Rockenbauch, K., Waldmann, R., 1998. Fazies, Diagenese und Reservoirentwicklung des Zechstein 2−Karbonats (Ober−Perm) in Nordostdeutschland. Geol. Jahrb., A (149), 81–113.

Taylor, S.R., McLennan, S.M., 1985. The Continental Crust: its Composition and Evolution. Blackwell Scientific, Oxford. 312 pp.

Truesdell, A.H., Hulston, J.R., 1980. Isotopic evidence in environments of geothermal systems. In: Fritz, P., Fontes, J.Ch. (Eds.), Handbook of Environmental Isotope Geochemistry: I. The Terrestrial Environment, A. Elsevier, Amsterdam, pp. 179–226.

Veizer, J., Hoefs, J., 1976. The nature of $^{18}O/^{16}O$ and $^{13}C/^{12}C$ secular trends in sedimentary carbonate rocks. Geochim. Cosmochim. Acta 40, 1387–1395.

Veizer, J., Holser, W.T., Wilgus, C.K., 1980. Correlation of $^{13}C/^{12}C$ and $^{34}S/^{32}S$ secular variations. Geochim. Cosmochim. Acta 44, 579–587.

Veizer, J., Fritz, P., Jones, B., 1986. Geochemistry of Brachiopods: oxygen and carbon isotopic records of Paleozoic oceans. Geochim. Cosmochim. Acta 50, 1679–1696.

Veizer, J., Ala, D., Azmy, K., Bruckschen, P., Buhl, D., Bruhn, F., Carden, G.A.F., Diener, A., Ebneth, S., Godderis, Y., Jasper, T., Korte, C., Pawellek, F., Podlaha, O.G., Strauss, H., 1999. $^{87}Sr/^{86}Sr$, $\delta^{13}C$ and $\delta^{18}O$ evolution of Phanerozoic seawater. Chem. Geol. 161, 59–88.

Walshaw, R.D., Menuge, J.F., 1998. Dating of crustal fluid flow by the Rb−Sr isotopic analysis of sphalerite; a review. In: Parnell, J. (Ed.), Dating and Duration of Fluid Flow and Fluid−Rock Interaction, Geological Society Special Publications, vol. 144, pp. 137–143.

Walters, L.J., Claypool, G.E., Choquette, P.W., 1972. Reaction rates and ^{18}O variation for the carbonate− phosphoric acid preparation method. Geochim. Cosmochim. Acta 36, 129–149.

Wedepohl, K.H., Delevaux, M.H., Doe, B.R., 1978. The potential source of lead in the Permian Kupferschiefer bed of Europe and some selected Paleozoic mineral deposits in the Federal Republic of Germany. Contrib. Mineral. Petrol. 65, 273–281.

Whelan, T., Bernard, B.B., Brooks, J.M., 1978. Carbon isotope variations in total carbon dioxide and methane from interstitial waters of nearshore sediments. N.Z. Dep. Sci. Ind. Res. Bull. 220, 39–47.

Whiticar, M.J., Faber, E., Schoell, M., 1986. Biogenic methane formation in marine and freshwater environments: CO_2 reduction vs. acetate fermentation− isotope evidence. Geochim. Cosmochim. Acta 50, 693–709.

Yalcin, M.N., Littke, R., Sachsenhofer, R.F., 1997. Thermal history of sedimentary basins. In: Welte, D.H., Horsfield, B., Baker, D.R. (Eds.), Petroleum and Basin Evolution. Springer, Berlin, pp. 71–166.

Zhang, J., Nozaki, S.M., 1998. Behaviour of rare earth elements in seawater at the ocean margin: a study along the slopes of Sagami and Nankai Troughs near Japan. Geochim. Cosmochim. Acta 62, 1307–1317.